

Hot Leptogenesis

Michael J. Baker,^a Ansh Bhatnagar,^b Djuna Croon,^b Jessica Turner^b

^a*Department of Physics, University of Massachusetts Amherst, MA 01003, USA*

^b*Institute for Particle Physics Phenomenology, Department of Physics, Durham University, Durham DH1 3LE, U.K.*

E-mail: mjbaker@umass.edu, ansh.bhatnagar@durham.ac.uk,
djuna.l.croon@durham.ac.uk, jessica.turner@durham.ac.uk

ABSTRACT: We investigate a class of leptogenesis scenarios in which the sector containing the lightest right-handed neutrino establishes kinetic equilibrium at a temperature $T_{N_1} > T_{\text{SM}}$, where T_{SM} is the temperature of the Standard Model sector. We study the reheating processes which realise this “hot leptogenesis” and the conditions under which kinetic and chemical equilibrium can be maintained. We derive and solve two sets of evolution equations, depending on the presence of chemical equilibrium within the hot sector, and numerically solve these for benchmark scenarios. We compare the viable parameter space of this model with standard leptogenesis scenarios with a thermal initial condition and find that hot leptogenesis resolves the neutrino and Higgs mass fine-tuning problems present in the standard scenario.

Contents

1	Introduction	2
2	Hot Leptogenesis from Inflaton Decays	3
3	A Model of Hot Leptogenesis	7
3.1	Kinetic and Chemical Equilibria	7
3.1.1	Condition 1 – Two Decoupled Sectors	9
3.1.2	Condition 2 – Kinetic Equilibrium within the Hot Sector	10
3.1.3	Condition 3 – Chemical Equilibrium Within the Hot Sector	11
3.2	Cosmology of the Scalar ϕ	12
3.3	Summary	13
4	Tracking the Evolution of the Hot and SM Sectors	13
4.1	N_1 in Kinetic and Chemical Equilibrium	15
4.2	N_1 in Kinetic Equilibrium Only	16
5	Results	18
5.1	N_1 in Kinetic Equilibrium Only	20
5.2	N_1 in Kinetic and Chemical Equilibrium	23
5.3	Further Scenarios	24
6	Conclusions	25
A	Cross-Sections, Decay Rates and Thermal Averaging	26
A.1	Cross-Sections and Decay Rates	26
A.2	Thermal Averaging	27
B	Fine-Tuning	28

1 Introduction

The observed neutrino masses can elegantly be explained by a seesaw mechanism. In the type-I seesaw mechanism [1–4], at least two Majorana right-handed neutrinos (RHNs) are added to the Standard Model (SM):

$$\mathcal{L} \supset i\bar{N}_i \not{\partial} N_i - \frac{1}{2} m_{N_i} \bar{N}_i^c N_i - Y_{\alpha i} \bar{L}_\alpha \tilde{\Phi} N_i + \text{h.c.}, \quad (1.1)$$

where i (α) denotes RHN generational (lepton flavour) indices and are summed over, the Yukawa matrix is given by Y and the leptonic and Higgs doublets are given by $L^T = (\nu_L^T, l_L^T)$ and Φ , respectively, with $\tilde{\Phi} = i\sigma_2\Phi$. Once the Higgs acquires a vacuum expectation value, the light neutrino masses are generated.

Besides providing a simple explanation for light neutrino masses, the type-I seesaw mechanism can also account for the observed baryon asymmetry via thermal leptogenesis [5]. In this scenario, a lepton asymmetry is produced through out-of-equilibrium and CP -violating decays of the RHNs [6–8]. This lepton asymmetry is then converted into a baryon asymmetry via electroweak sphalerons. Most leptogenesis calculations assume that the N_1 particles are in kinetic equilibrium with the Standard Model bath and inherit a thermal distribution with temperature T_{SM} . For parameter choices which reproduce the observed neutrino masses, the heavier right-handed neutrinos, N_2 and N_3 , are typically in both kinetic and chemical equilibrium with the SM thermal bath [9].

While the standard leptogenesis mechanism can successfully generate neutrino masses consistent with data along with the observed baryon asymmetry, it typically leads to a tension [10] between the Davidson-Ibarra bound [11] (a lower bound on the RHN masses, to achieve sufficient baryon asymmetry generation) and the Vissani bound [12] (an upper bound on the RHN masses, to avoid fine-tuning of the SM Higgs mass). Furthermore, successful leptogenesis comes at the cost of an accidental cancellation between the tree and one-loop contributions to the light neutrino mass matrix [13]. Resonant leptogenesis [14], characterised by significantly lighter RHNs with a highly degenerate mass spectrum that enhances CP asymmetry during their decays, provides a way to lower the leptogenesis scale while addressing fine-tuning issues in both the Higgs and neutrino mass matrices.

In this work, we present an alternative solution to these tensions, where N_1 has a higher temperature, T_{N_1} , than the SM particles. This leads to a larger number density of N_1 particles, which generate a larger baryon asymmetry after they decay. This scenario has previously been considered in Ref. [9], where an enhancement of up to ~ 50 times the standard leptogenesis baryon asymmetry can be obtained (the maximum exists because above some temperature the N_1 particles dominate the energy density of the universe). Ref. [9] requires a connection to thermal dark matter and concludes that resonant leptogenesis is still required to produce the observed baryon asymmetry. In this work, we drop the connection to dark matter and show that non-resonant leptogenesis can produce the observed baryon asymmetry while remaining natural. Schematically, the scenario is depicted in fig. 1. We will be interested in $T_{\text{SM}} < T_{N_1}$, and take the dominant coupling between the two sectors to be the one responsible for N_1 decay. Additional particles are needed

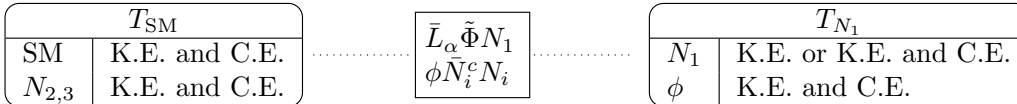


Figure 1: Field content and the temperatures of the sectors in hot leptogenesis, along with whether they are in kinetic and chemical equilibrium (K.E. and C.E.) or only kinetic equilibrium (K.E.) around the time of N_1 decay. The dominant coupling connecting the two sectors is taken to be the one responsible for N_1 decay. The scalar field ϕ , which keeps N_1 in kinetic equilibrium, may also mediate a coupling between N_1 and $N_{2,3}$ (and also between N_1 and the SM Higgs, not shown). Particles of the scalar field ϕ may or may not be present at the time of N_1 decay, depending on whether m_ϕ is much greater than T_{N_1} or not.

to realise equilibrium within the hot sector. We quantitatively demonstrate that this can be realised by introducing a new scalar, ϕ , which is primarily responsible for mediating the self-interactions of N_1 . Within this setup, we consider two regimes. In the first, N_1 is only in kinetic equilibrium during N_1 decay (so N_1 particles can exchange energy between themselves, but there are no number-changing processes that are sufficiently fast to realise chemical equilibrium). In the second, N_1 is in both kinetic and chemical equilibrium with itself and ϕ (similar to the regime considered in Ref. [9]). That is, they are both in thermal equilibrium in the hot sector during N_1 decay.

In section 2 we first motivate this setup, showing that it can be a consequence of inflaton decays. In section 3 we determine the regions of parameter space in our toy model where the two scenarios (N_1 in kinetic or kinetic and chemical equilibrium) are realised and discuss the cosmological constraints on the ϕ particle. In section 4 we derive the relevant Boltzmann equations to track the evolution of the sectors and compute the resulting baryon asymmetry. We present and discuss our results in section 5 and conclude in section 6.

2 Hot Leptogenesis from Inflaton Decays

While the mechanism of inflation is not yet determined, as a proof of principle we here discuss one plausible scenario. The origin of two sectors with similar, but different, temperatures could be explained by an inflaton that couples with different strengths to the particles within each sector. Assuming perturbative reheating, the reheating temperature in each sector is approximately,¹

$$T_R \approx \sqrt{\Gamma M_{\text{Pl}}}, \quad (2.1)$$

where Γ is the inflaton decay rate to particles within that sector and $M_{\text{Pl}} = 1.22 \times 10^{19}$ GeV is the Planck mass. The decay rate of an inflaton σ , with mass m_σ , to decay to particle

¹Note that for efficient parametric resonance, the relation is more complicated. Parametric resonance is suppressed for inflaton decays to fermions due to Pauli blocking.

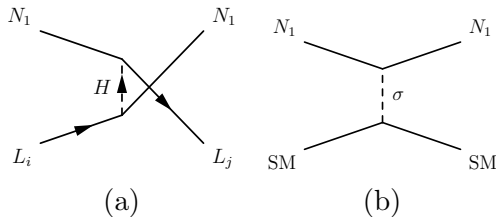


Figure 2: Feynman diagrams showing the (a) Higgs- and (b) inflaton-mediated processes which could thermalise the hot and SM sectors. All Standard Model particles are denoted simply by SM.

species i , with mass m_i , is approximately

$$\Gamma_i \approx \frac{y^2 m_\sigma}{8\pi}, \quad (2.2)$$

for $m_i \ll m_\sigma$ and where y is the coupling of the inflaton to the particle. For an inflaton mass $m_\sigma \sim 10^{13}$ GeV, the reheating temperature is then $T_R \sim y \times 10^{15}$ GeV, and the ratio of temperatures between the two sectors is

$$\kappa \equiv \frac{T_{N_1}}{T_{\text{SM}}} \approx \sqrt{\frac{\Gamma_{N_1}}{\Gamma_{\text{SM}}}} \approx \frac{y_{N_1}}{y_{\text{SM}}}, \quad (2.3)$$

where y_{N_1} (y_{SM}) is the largest coupling of the inflaton to particles in the hot (SM) sector. As long as the two sectors cannot efficiently exchange energy, $y_{\text{SM}} < y_{N_1}$ will typically lead to $T_{\text{SM}} < T_{N_1}$. While other factors can impact the precise value of κ , such as the spin of the daughter particles or other degrees of freedom with smaller couplings to σ , the fact that y_{N_1} and y_{SM} are not constrained by experiment mean that a wide range of values of κ is plausible.

If there is only a weak coupling between the two sectors, they will not thermalise before the hot N_1 particles decay into particles in the SM sector. A weak coupling means that leptogenesis will operate in the weak washout regime and ensures that scattering processes (such as those shown in fig. 2 (a)) are out-of-equilibrium before N_1 decays. In the case of strong washout, there are rapid interactions between the N_1 particles and the SM sectors which would cause the two sectors to thermalise. It is also important that the inflaton itself does not thermalise the hot and SM sectors through the process shown in fig. 2 (b). To avoid this, we require the scattering rate between SM particles and N_1 particles to be slower than the Hubble rate. Taking a simple Yukawa coupling between the inflaton and N_1 ,

$$\mathcal{L} \supset \frac{1}{2} y_{N_1} \sigma \bar{N}_1^c N_1, \quad (2.4)$$

and assuming that the dominant inflaton-SM coupling is a universal Yukawa coupling to all SM fermions,

$$\mathcal{L} \supset y_{\text{SM}} \sigma \sum_{f \in \text{SM}} \bar{\psi}_f \psi_f, \quad (2.5)$$

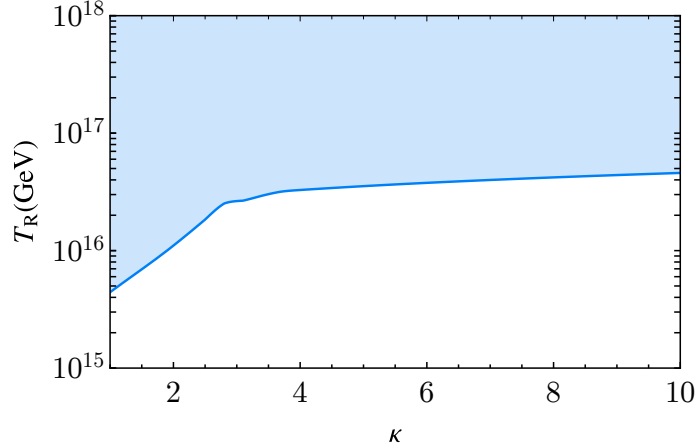


Figure 3: Upper bound on the reheating temperature in the hot sector from the requirement that inflaton-mediated elastic scattering does not realise kinetic equilibrium between the hot and SM sectors. In this plot we take $m_{N_1} = 10^7$ GeV and $m_\sigma = 10^{13}$ GeV.

we require

$$\Gamma_{N_1 \text{ SM} \rightarrow N_1 \text{ SM}} = \max(n_{N_1}, n_{\text{SM}}) \langle \sigma v \rangle < H, \quad (2.6)$$

where n_{N_1} and n_{SM} are the relevant number densities and $\langle \sigma v \rangle$ is the thermally averaged elastic cross-section between N_1 and the SM fermions via an inflaton mediator. When the inflaton decays, the SM particles quickly reach thermal equilibrium so $n_{\text{SM}} = n_{\text{SM}}^{\text{eq}}(T_{\text{SM}})$. We assume that some unspecified UV particles also allow N_1 to reach thermal equilibrium with itself around the reheating temperature, so that $n_{N_1} = 3\zeta(3)g_{N_1}T_{N_1}^3/4\pi^2$ where $g_{N_1} = 2$ is the number of degrees of freedom of N_1 , but that these reactions rates fall below the Hubble rate before N_1 starts to decay (see section 4). The cross-section for inflaton-mediated N_1 –SM scatterings is

$$\sigma = \frac{y_{\text{SM}}^2 y_{N_1}^2}{4\pi s^2 (m_\sigma^2 + s)} \left[s (2m_\sigma^2 - 4m_{N_1}^2 + s) - 2 (2m_{N_1}^2 - m_\sigma^2) (m_\sigma^2 + s) \log \left(\frac{m_\sigma^2}{m_\sigma^2 + s} \right) \right], \quad (2.7)$$

where s denotes the centre-of-mass energy, m_{N_1} the mass of N_1 and we have assumed $m_f \ll m_{N_1}, m_\sigma$. The thermal averaging for this process is discussed in appendix A.1. For a universe consisting of two decoupled relativistic sectors with temperature ratio κ , the Hubble rate is given by

$$H = \sqrt{\frac{8\pi^3}{90} (g_{\text{SM}}^* + g_{N_1}^* \kappa^4)} \frac{T_{\text{SM}}^2}{M_{\text{Pl}}}, \quad (2.8)$$

where g_{SM}^* and $g_{N_1}^*$ denote the effective number of degrees of freedom in the Standard Model and hot sectors, respectively. The relative sizes of g_{SM}^* and $g_{N_1}^* \kappa^4$ determine which sector dominates the energy density of the Universe. For energies above the electroweak scale, with $g_{\text{SM}}^* = 106.75 + 4$ and assuming $g_{N_1}^* = 2$, the SM sector dominates the Universe's energy density for $\kappa \lesssim 2.7$, while the hot sector dominates for $2.7 \lesssim \kappa$.

Given eqs. (2.6) to (2.8), we can determine the maximum value of $y_{\text{SM}y_{N_1}}$ that ensures that the inflaton does not thermalise the two sectors. For a given κ , this gives an upper bound on the reheating temperature of the hot sector. For chaotic inflation, which fixes $m_\sigma \approx 10^{13}$ GeV, and using $m_{N_1} = 10^7$ GeV as our benchmark value, the white region of fig. 3 shows the viable reheating temperatures of the hot sector as a function of κ . In the blue region, inflaton-mediated interactions will thermalise the two sectors, so that $T_{\text{SM}} \approx T_{N_1}$ and standard leptogenesis would proceed. We find that for the two sectors to remain decoupled, we require $T_R \lesssim 10^{17}$ GeV, with a slight reduction when $\kappa \lesssim 3.8$ (where $n_{\text{SM}} \lesssim n_{N_1}$). We will be interested in N_1 masses around 10^7 GeV, motivated by the Vissani bound limiting $m_{N_1} \lesssim 7.4 \times 10^7$ GeV for the Higgs mass parameter μ^2 to remain below 1 TeV^2 [12]. Thus, the reheating temperature in the hot sector can be well above the right-handed neutrino masses.

As mentioned above, the inflaton couplings to the different sectors are experimentally unconstrained. As such, κ can in principle take a wide range of values. Some limiting scenarios often studied in the literature are:

1. The inflaton decays exclusively to N_1 [15–20], corresponding to an initial $n_{\text{SM}} = 0$ and $\kappa \rightarrow \infty$. Such a scenario is typically studied in the context of non-thermal leptogenesis, where the assumption is that $T_R \ll m_{N_1}$ and that the N_1 decay happens immediately after the inflaton decay. For example, Ref. [16] assumes that perturbative inflaton decay is kinematically forbidden, i.e., $m_\phi < 2m_{N_1}$ so that the only relevant decay are through strong parametric resonance (overcoming Pauli-blocking of fermions). Ref. [17] studies perturbative inflaton decay into N_1 , but with $100T_R \lesssim m_{N_1}$ such that the N_1 particles are always out of kinetic and chemical equilibrium, making leptogenesis non-thermal. In this latter scenario, N_1 and the inflaton have similar masses, which is somewhat of a coincidence of scales. The inflaton decaying exclusively to N_1 was first studied away from the limit $T_R \ll m_{N_1}$ in Ref. [20]. Without a self-interaction in the hot sector, the N_1 distribution after inflaton decay is non-thermal, and the Universe becomes radiation-dominated only after N_1 decay, complicating numerical analysis. In our work, we will assume $m_{N_i} \ll T_R$ and the presence of an N_1 self-interaction, so the N_1 particles rapidly achieve a thermal distribution.
2. The inflaton decay leads to $\kappa \approx 1$. When we take the case that N_1 are in kinetic and chemical equilibrium with themselves, see section 3.1.3, our calculations with $\kappa = 1$ are comparable to the standard leptogenesis scenario with a thermal initial condition.
3. The inflaton decays only to the SM, corresponding to $\kappa \rightarrow 0$. This scenario corresponds to standard leptogenesis with a vanishing initial abundance of N_1 . Since we are interested in increasing the baryon asymmetry compared to standard leptogenesis by increasing the number density of N_1 particles in a sector that is hotter than the SM sector, we will not study $\kappa < 1$.

In summary, we see that it is plausible for a simple model of inflation to lead to two decoupled sectors at a similar but different temperature, with a reheating temperature

that is significantly above the right-handed neutrino masses. In what follows, we will take this as a starting point and we will study two different scenarios in the regime $1 \lesssim \kappa$.

3 A Model of Hot Leptogenesis

While there are many possible realisations of the scenario we discuss, for concreteness we study a toy model consisting of the SM plus N_2 and N_3 at temperature T_{SM} and a hot sector containing N_1 and a real scalar ϕ at temperature T_{N_1} . The lightest right-handed neutrino, N_1 , will decay to produce a lepton asymmetry which ultimately produces the baryon asymmetry, while ϕ will mediate interactions in the hot sector. We will consider two cases: that around the time of N_1 decay either N_1 is only in kinetic equilibrium with itself, or N_1 is in both kinetic and chemical equilibrium with itself. In this section, we find the regions of parameter space which exhibit these two cases.

The relevant interaction Lagrangian terms in our toy model are,

$$\begin{aligned} \mathcal{L} \supset & -Y_{\alpha i} \bar{L}_\alpha \tilde{\Phi} N_i + \text{h.c.} \\ & -y_\phi^i \phi \bar{N}_i^c N_i - \frac{m_\phi^2}{2} \phi^2 - \frac{\lambda_3 m_\phi}{3!} \phi^3 - \frac{\lambda}{4!} \phi^4, \end{aligned} \quad (3.1)$$

where $i \in \{1, 2, 3\}$ and $\alpha \in \{e, \mu, \tau\}$. The Yukawa matrix, $Y_{\alpha i}$, is parametrised using the Casas-Ibarra parameterisation [21], $Y = \frac{1}{v} U \sqrt{M_\nu} R^T \sqrt{M_N}$, where $v = 174 \text{ GeV}$ is the vacuum expectation value of the Higgs, U is the leptonic mixing matrix, M_ν (M_N) is the diagonal light (heavy) neutrino mass matrix and R is a complex, orthogonal matrix. We discuss our specific choice of benchmark point for $Y_{\alpha i}$ in section 5. We assume that the ϕ^3 term is small enough that ϕ does not obtain a vacuum expectation value ($m_\phi^2 > 0$ and $\lambda_3 < \sqrt{3\lambda}$). While in principle there are also cubic and quartic couplings with the SM Higgs, $\phi|\Phi|^2$ and $\phi^2|\Phi|^2$, we assume that these are small enough to keep the two sectors out of thermal contact. Although the inflaton could potentially play the role of ϕ , we do not study this possibility and instead introduce a new scalar particle. As noted in the introduction, standard leptogenesis leads to fine-tuning in the SM Higgs mass [10, 12] and/or in the light neutrino masses [13]. The relevant expressions can be found in these references and the fine-tuning measures we use are given in appendix B.

3.1 Kinetic and Chemical Equilibria

We first consider the expected phase space distribution of N_1 in different regions of the parameter space of this model. When N_1 is in kinetic and chemical equilibrium, it will have a Fermi-Dirac phase space distribution function, with zero chemical potential. When N_1 is only in kinetic equilibrium, its phase space distribution assumes the same form but will be normalised so that the number density of particles, n_{N_1} , is not fixed to the equilibrium number density,

$$f_{N_1} = \frac{n_{N_1}}{n_{N_1}^{\text{eq}}} f_{N_1}^{\text{eq}}. \quad (3.2)$$

Another possibility is that N_1 may have been in kinetic equilibrium at some point after inflaton decay but came out of kinetic equilibrium sometime before N_1 decay. We do not analyse this case in detail, which would require the tracking of individual momentum modes, but we briefly discuss the expected applicability of our results to this scenario. Finally, if the N_1 particles were never in kinetic equilibrium, their momentum would be spiked around half the inflaton mass. We will not consider this case here.

There are a variety of processes to consider to determine which particles are in kinetic or chemical equilibria with themselves or each other. The two sectors are necessarily coupled by the Lagrangian term responsible for N_1 decay, and potentially also by ϕ mediated processes. The new scalar ϕ can keep N_1 in kinetic equilibrium with itself through s -, t - and u -channel scattering processes, and if ϕ is not too much heavier than N_1 then number-changing interactions could also keep N_1 in chemical equilibrium with itself. We now find the regions of parameter space where the following conditions hold:

1. All elastic scattering processes between the hot and SM sectors are slower than the Hubble expansion rate.
2. Elastic $N_1 N_1 \leftrightarrow N_1 N_1$ scattering processes are faster than the Hubble expansion rate.
3. Number changing processes of both N_1 and ϕ are faster than the Hubble expansion rate.

Condition 1 ensures that the two sectors are decoupled, allowing each sector to maintain independent temperatures. Condition 2 ensures that N_1 is in kinetic equilibrium with itself, resulting in a Fermi-Dirac-shaped phase space distribution function. In our analyses, we will ensure that these two conditions always hold. If Condition 3 is satisfied, N_1 will be in both kinetic and chemical equilibrium, achieving an equilibrium number density. It is important to note that chemical equilibrium requires processes that can independently change the comoving number densities of N_1 and ϕ ; for example, the process $2N_1 \leftrightarrow 2\phi$ alone is not sufficient.

The Hubble rate in this model is given by

$$H = \frac{1}{\sqrt{3}M_{\text{pl}}} \sqrt{\frac{\pi^2}{30} g_*^{\text{SM}}(T_{\text{SM}}) T_{\text{SM}}^4 + \rho_{N_1} + \rho_{N_2} + \rho_{N_3} + \rho_\phi}, \quad (3.3)$$

where for N_i and ϕ

$$\rho = \frac{n}{n^{\text{eq}}} \rho^{\text{eq}} = \frac{n}{n^{\text{eq}}} \frac{g}{2\pi^2} T^4 J_\pm \left(\frac{m}{T} \right), \quad (3.4)$$

where

$$J_\pm(z) = \int_0^\infty d\xi \frac{\xi^2 \sqrt{\xi^2 + z^2}}{\exp[\sqrt{\xi^2 + z^2}] \pm 1}, \quad (3.5)$$

with a plus sign for fermion, a negative sign for bosons and where $\xi = |\vec{p}|/T_{N_1}$. For N_2 and N_3 , which have a vanishing initial condition but approach their equilibrium energy densities

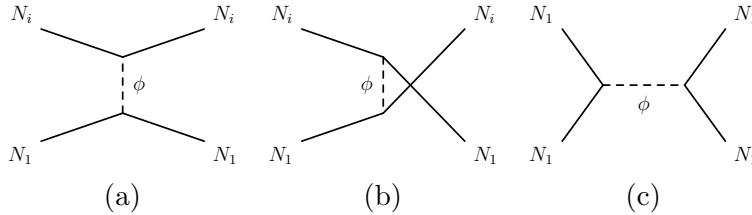


Figure 4: Feynman diagrams showing the processes which may put N_1 in kinetic equilibrium with the SM bath before N_1 decays ((a) and (b) with $i \in \{2, 3\}$), which would set $T_{\text{SM}} = T_{N_1}$, and with itself ((a), (b) and (c) with $i = 1$).

throughout the evolution, for computational simplicity we approximate their contribution to the energy density as relativistic fermions in thermal equilibrium for $m_{N_{2,3}} < T_{\text{SM}}$ and we neglect their contribution otherwise. We have checked that this approximation does not affect our final results.

3.1.1 Condition 1 – Two Decoupled Sectors

For the hot sector to remain thermally decoupled from the SM sector, we require that the decay rate of N_1 to SM particles is slower than the Hubble rate at $T_{N_1} \gtrsim m_{N_1}$. For $m_{N_1} \approx 10^7$ GeV this gives $Y_{\alpha 1} \lesssim 10^{-5}$. This condition ensures leptogenesis proceeds in the weak washout regime and that the two sectors do not thermalise via inverse decays or $N_1 \text{SM} \rightarrow N_1 \text{SM}$ scatterings [22, 23] before N_1 decays [9].

Beyond the direct coupling of N_1 with the SM plasma, it is possible that the ϕ -mediated coupling between N_1 and the heavier N_2 and N_3 (which will be thermally produced in the SM sector) may thermalise the two sectors via scattering processes shown in fig. 4 (a) and (b). We need to check that the interaction rate per N_1 particle and per $N_{2,3}$ particle is slower than the Hubble rate. For $n_{N_1} \approx n_{N_1}^{\text{eq}}$ we will have $n_{N_{2,3}} < n_{N_1}$ since $m_{N_1} < m_{N_{2,3}}$ and $T_{\text{SM}} < T_{N_1}$, so the rate per N_1 particle is slower than the rate per $N_{2,3}$ particle. We therefore only need to check the rate per $N_{2,3}$ particle. The two sectors will then not thermalise as long as

$$n_{N_1} \langle \sigma v \rangle_{N_1 N_{2,3} \rightarrow N_1 N_{2,3}} < H, \quad (3.6)$$

where the cross-section is given in eq. (A.1), the thermal averaging is given in eq. (A.11) and the Hubble rate is given in eq. (3.3). Here, and for the remaining rate calculations, in this section we approximate $n_{N_1}^{\text{eq}} \approx n_{N_1}$. In principle, this could be modified when chemical equilibrium does not hold. This would lead to a proportional shift in the rates calculated here. Thus, our conclusions should be taken as a guide rather than precise statements for the kinetic equilibrium-only scenario. However, it is a good approximation for the kinetic equilibrium-only cases we consider.

We may expect the $N_1 - \phi$ Yukawa coupling y_ϕ^1 to be a similar order to y_ϕ^2 and y_ϕ^3 since the right-handed neutrino masses are all at a similar scale (although note that we do not discuss the origin of the right-handed neutrino masses here and do not assume that ϕ is a Majoron). The blue region above the dashed blue contour in fig. 5 shows where the rate

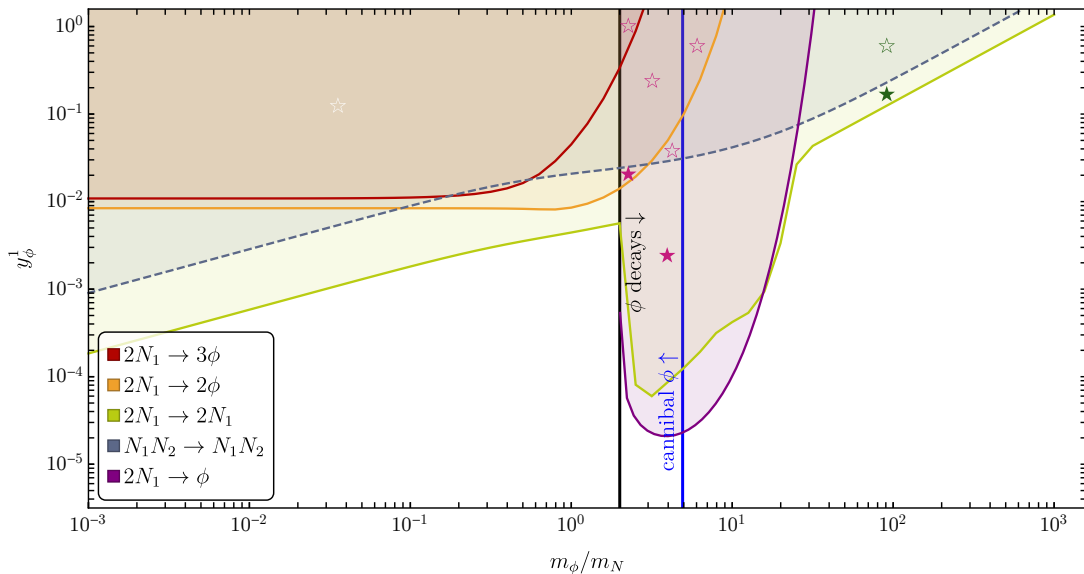


Figure 5: Minimal value of y_ϕ^1 such that the various interaction rates are greater than Hubble around the time of decay, $T_{N_1} = m_{N_1} = 10^7$ GeV. We have assumed that Hubble is dominated by the SM as it is right after the decays and that $\lambda = 0.8$. Assuming $y_\phi^1 = y_\phi^2$, the scattering process $N_1 N_2 \leftrightarrow N_1 N_2$ will thermalise the SM and hot sectors in the blue region above the dashed blue contour. To the left of the black line the ϕ abundance will deplete with the N_1 abundance. To the left of the blue line (labelled “cannibal ϕ ”) the cannibal process $2\phi \leftrightarrow 3\phi$ is effective. The pink (green) stars indicate example points in the toy model parameter space where kinetic and chemical (only kinetic) equilibrium can be achieved, where open stars require $y_\phi^2, y_\phi^3 \ll y_\phi^1$. The white star shows a point where the cosmology of ϕ would need to be carefully considered.

of this process is greater than the Hubble rate at the time of N_1 decay assuming $y_\phi^1 = y_\phi^2$. That is, where condition 1 is not satisfied. However, this bound can be relaxed, without affecting any other phenomenology, by taking $y_\phi^2 \ll y_\phi^1$. Throughout this work, we consider the parameter space where the $N_1 N_{2,3} \leftrightarrow N_1 N_{2,3}$ scattering rate is less than the Hubble expansion rate to ensure the two sectors do not thermalise with each other.

3.1.2 Condition 2 – Kinetic Equilibrium within the Hot Sector

The processes shown in fig. 4 (a) and (b) along with an extra s -channel process, fig. 4 (c), will keep N_1 in kinetic equilibrium with itself if condition 2 is satisfied,

$$n_{N_1} \langle \sigma v \rangle_{2N_1 \rightarrow 2N_1} > H, \quad (3.7)$$

where the cross-section is given in eq. (A.2) and the thermal averaging is given by eq. (A.7). The green region in fig. 5 shows where condition 2, or eq. (3.7), is satisfied. We see that there is a minimum value of y_ϕ^1 for a given m_ϕ/m_{N_1} . When $2m_{N_1} \lesssim m_\phi$ there is a resonant enhancement as the ϕ propagator in fig. 4 (c) can go on-shell.

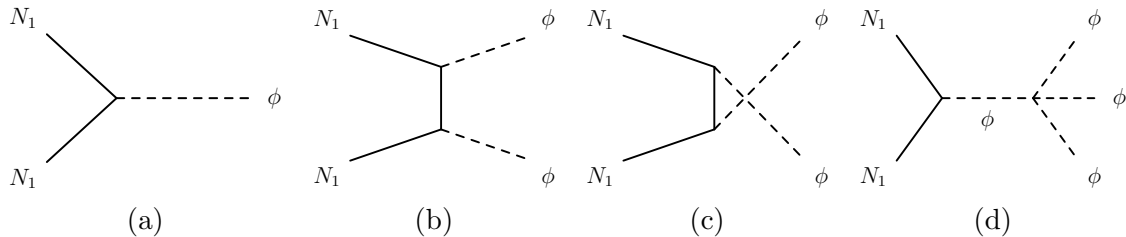


Figure 6: Feynman diagrams showing processes which could keep N_1 in chemical equilibrium with the hot sector.

3.1.3 Condition 3 – Chemical Equilibrium Within the Hot Sector

If there are fast number-changing interactions, such as those shown in fig. 6, N_1 could also be in chemical equilibrium in the hot sector. Chemical equilibrium requires processes which can increase (or decrease) both the comoving number densities of N_1 and ϕ at the same time. This could, for instance, be a combination of $2N_1 \leftrightarrow \phi$ and $2N_1 \leftrightarrow 2\phi$, or either of those along with $2\phi \leftrightarrow 3\phi$. If these processes are faster than the Hubble rate we may assume that n_{N_1} is simply given by $n_{N_1}^{\text{eq}}$, which simplifies the analysis. This is a version of the scenario considered in [9] (see, e.g., their eq. 2.19), where the hot sector was populated by the decay of dark matter. If only one of these processes is faster than the Hubble rate, neither N_1 nor ϕ can be assumed to be in chemical equilibrium and their abundances should be tracked dynamically.

N_1 and ϕ also both need to be in chemical equilibrium in the hot sector, so we technically need to check the rate per N_1 particle and the rate per ϕ particle. However, since $n_\phi^{\text{eq}} < n_{N_1}^{\text{eq}}$ at $T_{N_1} = m_{N_1}$ for all ϕ masses, we only need to check the rate per N_1 particle. The purple region in fig. 5 shows where $\phi \leftrightarrow 2N_1$ decays and inverse decays, fig. 6 (a), occur faster than the Hubble rate,

$$\langle \Gamma_{\phi \rightarrow 2N_1} \rangle \frac{n_\phi^{\text{eq}}}{n_{N_1}^{\text{eq}}} = \Gamma_{\phi \rightarrow 2N_1} \frac{K_1(m_{N_1}/T_{N_1})}{K_2(m_{N_1}/T_{N_1})} \frac{n_\phi^{\text{eq}}}{n_{N_1}^{\text{eq}}} > H, \quad (3.8)$$

where the $\phi \rightarrow 2N_1$ decay rate is given in eq. (A.3) and K_1 and K_2 are modified Bessel functions of the second kind. We see that in the range $2m_{N_1} \lesssim m_\phi \lesssim 10m_{N_1}$ this rate is faster than the Hubble rate if $10^{-4} \lesssim y_\phi^1$, and for larger y_ϕ^1 this process can be relevant up to $m_\phi \approx 30m_{N_1}$.

Next, we consider the process $2\phi \leftrightarrow 3\phi$, which is independent of the coupling y_ϕ^1 . Choosing a representative $\lambda = 0.8$ and $\lambda_3 = 0.57\sqrt{3\lambda}$,² we find that the region left of the blue vertical line satisfies

$$n_\phi^2 \langle \sigma v^2 \rangle_{3\phi \rightarrow 2\phi} > H, \quad (3.9)$$

where we take the thermally averaged cross-section from Ref. [25]. We see that, for these parameters, this process is faster than Hubble for $m_\phi < 5m_{N_1}$. In what follows, when we

²This value, which is not the result of spontaneous symmetry breaking [24], is chosen to maximise the cross-section.

assume chemical equilibrium we will work in regions of parameter space where $2N_1 \leftrightarrow 2N_1$, $\phi \leftrightarrow 2N_1$ and $2\phi \leftrightarrow 3\phi$ are all faster than Hubble. However, we now briefly consider some other processes that could potentially be relevant.

The orange region in fig. 5 shows where the $2N_1 \leftrightarrow 2\phi$ processes, fig. 6 (b) and (c), are faster than the Hubble rate,

$$n_{N_1} \langle \sigma v \rangle_{2N_1 \rightarrow 2\phi} > H, \quad (3.10)$$

where the cross-section is given in eq. (A.4) and the thermal averaging is given in eq. (A.7). For $m_\phi \lesssim m_{N_1}$ this process is faster than Hubble if $10^{-2} \lesssim y_\phi^1$, while for heavier ϕ particles a larger coupling is required.

The process $2N_1 \leftrightarrow 3\phi$ can occur either via t -channel-like diagrams, where the cross-section is proportional to $(y_\phi^1)^6$ or via an s -channel type diagram, fig. 6 (d), whose cross-section is proportional $(y_\phi^1)^2 \lambda^2$. Since we are mostly interested in the region $y_\phi^1 \ll \lambda \approx 1$, where the t -channel processes will be suppressed, we show in red in fig. 5 the region where the s -channel process is faster than Hubble,

$$n_{N_1} \langle \sigma v \rangle_{2N_1 \rightarrow 3\phi} > H. \quad (3.11)$$

The cross-section for this process is given by eq. (A.5) and the thermal averaging is done using eq. (A.7). We see that this process is only faster than Hubble when $2N_1 \leftrightarrow 2\phi$ and $2\phi \leftrightarrow 3\phi$ are both faster than Hubble, so it does not create any new regions where chemical equilibrium for N_1 can be established (assuming similar values of λ_3 and λ to those chosen here).

Another number-changing process that could be relevant is $2\phi \rightarrow 4\phi$. However, for an n -body massless particle, the phase space factor goes as

$$PS^{(n)} \sim \frac{1}{2(4\pi)^{2n-3} \Gamma(n) \Gamma(n-1)}. \quad (3.12)$$

In comparison to the $2\phi \rightarrow 3\phi$ cross-section, there is a phase space suppression factor of $1/(192\pi^2)$. Therefore the ratio of the cross-sections goes as

$$\frac{\sigma_{2\phi \rightarrow 4\phi}}{\sigma_{2\phi \rightarrow 3\phi}} \sim \frac{\lambda^2}{192\pi^2 \lambda_3^2}. \quad (3.13)$$

This implies that the $2\phi \rightarrow 4\phi$ process is subdominant to $2\phi \rightarrow 3\phi$ as long as $\lambda \ll \sqrt{192\pi} \lambda_3 \approx 44\lambda_3$.

3.2 Cosmology of the Scalar ϕ

We finish this section with a discussion of the cosmology of the new scalar ϕ . If $m_\phi < 2m_{N_1}$, the hot sector will not deplete during N_1 decay and there will be a non-negligible abundance of ϕ , which will freeze out relativistically. While the scalar ϕ is not stable, its four-body decay (via two off-shell N_1 particles) is suppressed by $Y_{\alpha i}^4$. If ϕ couples to all three RHNs, we find that $Y_{\alpha i}$ is typically large enough such that the decay can be expected to deplete the sector before BBN. However, this will cause a large entropy dump which will wash out

the generated asymmetry to some extent. If ϕ only couples to N_1 , the smallness of $Y_{\alpha i}$ implies that ϕ is stable on a cosmological timescale. Because it freezes out relativistically, its large abundance will either give rise to a large contribution to ΔN_{eff} – the number of relativistic degrees of freedom at BBN – or an overproduction of (dark) matter, depending on its mass. We conclude that in our current model m_ϕ needs to be larger than $2m_{N_1}$.³

3.3 Summary

In summary, we see that there are many relevant processes and different possible regimes which can realise kinetic or kinetic and chemical equilibrium in the hot sector, even for our simple toy model. To ensure the SM and hot sectors remain decoupled we require that leptogenesis occurs in the weak washout regime, effectively limiting the size of the Yukawa coupling. From fig. 5 we see that, for $\lambda = 0.8$ and $\lambda_3 \sim \sqrt{3\lambda}$, we can assume that N_1 is in kinetic and chemical equilibrium with the hot sector around the time of N_1 decays if $2m_{N_1} < m_\phi < 5m_{N_1}$, $10^{-4} \lesssim y_\phi^1$ and $y_\phi^{2,3} \lesssim 10^{-2}$. For $\lambda \ll 1$ chemical equilibrium could be established through $\phi \leftrightarrow 2N_1$ and $2N_1 \leftrightarrow 2\phi$ (which requires $y_\phi^1 \gtrsim 10^{-2}$ and typically require $y_\phi^{2,3} \ll y_\phi^1$). When $30m_{N_1} \lesssim m_\phi$ and $y_\phi^{2,3} \lesssim 10^{-2} \lesssim y_\phi^1$ we can assume that N_1 is only in kinetic equilibrium. Both cases can also be realised for $m_\phi < 2m_{N_1}$, but in that case an entropy dump and/or washout would need to be carefully considered. We indicate with pink, green and white stars the regions where these conditions hold (see caption of fig. 5 for details).

4 Tracking the Evolution of the Hot and SM Sectors

In the simplest formulation, the leptogenesis kinetic equations operate in the one-flavoured regime, accounting for only a single flavour of charged lepton. This is a good approximation at very high temperatures ($T \gg 10^{12}$ GeV) when charged lepton Yukawa coupling processes are out of thermal equilibrium, resulting in a coherent superposition of the three flavour eigenstates. However, at lower temperatures (10^9 GeV $\ll T \ll 10^{12}$ GeV), the interaction rates proportional to the tau Yukawa couplings come into thermal equilibrium and can cause decoherence, necessitating a description in terms of two flavour eigenstates. In our case, leptogenesis occurs at even lower temperatures ($T < 10^9$ GeV), where interactions mediated by the muon have equilibrated. In these regimes, a density matrix formalism [26–30] provides a more comprehensive description than semiclassical Boltzmann equations, which do not include flavour oscillations in the lepton asymmetry. For this reason, we solve the density matrix equations which capture the time evolution of the RHN number densities in the hot and SM sectors, and the lepton asymmetry number density (which is promoted to a density matrix, $N_{\alpha\beta}$). As discussed in section 2, the Hubble expansion rate depends on the energy densities of both the hot and SM sectors. Since we track the energy density of both sectors, it will be convenient to evolve the density matrix equation as a

³An alternative possibility is the existence of an additional portal coupling (for example a coupling to the SM Higgs) through which the ϕ abundance can deplete. In this scenario, the washout effect from this decay needs to be carefully considered.

function of the scale factor, a , which is then

$$aH \frac{dN_{N_1}}{da} = -\Gamma_{D_1}(z_{N_1})N_{N_1} + \Gamma_{D_1}(z_{\text{SM}})N_{N_1}^{\text{eq}}, \quad (4.1)$$

$$aH \frac{dN_{N_2}}{da} = -\Gamma_{D_2}(z_{N_2}) \left(N_{N_2} - N_{N_2}^{\text{eq}} \right), \quad (4.2)$$

$$aH \frac{dN_{N_3}}{da} = -\Gamma_{D_3}(z_{N_3}) \left(N_{N_3} - N_{N_3}^{\text{eq}} \right), \quad (4.3)$$

$$\begin{aligned} aH \frac{dN_{\alpha\beta}}{da} &= \epsilon_{\alpha\beta}^{(1)} \left(\Gamma_{D_1}(z_{N_1})N_{N_1} - \Gamma_{D_1}(z_{\text{SM}})N_{N_1}^{\text{eq}} \right) - \frac{1}{2}W_1 \left\{ P^{(1)}, n \right\}_{\alpha\beta} \\ &+ \sum_{i=2}^3 \epsilon_{\alpha\beta}^{(i)} \Gamma_{D_i}(z_{N_i}) \left(N_{N_i} - N_{N_i}^{\text{eq}} \right) - \frac{1}{2}W_i \left\{ P^{(i)}, N \right\}_{\alpha\beta} \\ &- \Lambda_\tau \left[\begin{pmatrix} 1 & 0 & 0 \\ 0 & 0 & 0 \\ 0 & 0 & 0 \end{pmatrix}, \left[\begin{pmatrix} 1 & 0 & 0 \\ 0 & 0 & 0 \\ 0 & 0 & 0 \end{pmatrix}, N \right] \right]_{\alpha\beta} - \Lambda_\mu \left[\begin{pmatrix} 0 & 0 & 0 \\ 0 & 1 & 0 \\ 0 & 0 & 0 \end{pmatrix}, \left[\begin{pmatrix} 0 & 0 & 0 \\ 0 & 1 & 0 \\ 0 & 0 & 0 \end{pmatrix}, N \right] \right]_{\alpha\beta}, \end{aligned} \quad (4.4)$$

where i is a generation index, α, β are lepton flavour indices, N_{N_i} and $N_{\alpha\beta}$ are the comoving number density of N_i and the $B-L$ asymmetry for lepton flavour indices α, β , respectively, $\Gamma_{D_i} = \Gamma_{D_i}^0 \langle m_{N_i}/E_{N_i} \rangle$ are the thermally averaged decay rates of N_i where we assume Maxwell-Boltzmann statistics with $\langle m_{N_i}/E_{N_i} \rangle = K_1(z_{N_i})/K_2(z_{N_i})$. For the N_1 decay, we thermally average over the hot sector using the variable $z_{N_1} = m_{N_1}/T_{N_1}$ while for the N_1 inverse decays from the SM, and for N_2 and N_3 , we thermally average over the Standard Model sector using the variables $z_{\text{SM}} = m_{N_1}/T_{\text{SM}}$ and $z_{N_{2,3}} = m_{N_{2,3}}/T_{\text{SM}}$ respectively. The equilibrium abundance of N_i is denoted as N_i^{eq} and the initial abundance of N_1 is $N_{N_1} \propto \kappa^3$. The initial abundance for N_2 and N_3 are assumed to be vanishing. The washout terms, which remove the lepton asymmetry produced by decays of N_1 in the hot sector, are denoted by W_i . We remind the reader that when the hot and visible sectors remain decoupled before N_1 decays, the washout is weak. The decay asymmetry (between RHNs decaying to leptonic and Higgs doublet versus the CP-conjugate process) generated by the decays of N_i is given by the CP-asymmetry matrix $\epsilon_{\alpha\beta}^{(i)}$ [6, 28, 30, 31]. Λ_τ (Λ_μ) denote the thermal widths of the tau (muon) charged leptons, which is obtained from the imaginary part of the self-energy correction to the lepton propagator in the plasma. Finally, $P_{\alpha\beta}^{(i)} \equiv c_{i\alpha}c_{i\beta}^*$ where $c_{i\alpha} = Y_{\alpha i}/\sqrt{(YY)_{ii}}$ denote projection matrices which describe how a given flavour of lepton is washed out. We note that this equation describes both the decays of N_1 from the hot sector into the SM and the possible inverse decays from the SM into the hot sector, as well as the SM washout processes. We note that while we include the evolution of the RHNs N_2 and N_3 for completeness, their contribution to the lepton asymmetry compared to N_1 is small. To compute the final lepton asymmetry one solves eq. (4.1) for $z_{N_1} \gg 1$ and takes the trace of the $N_{\alpha\beta}$ matrix, $N_{B-L}^f = \text{Tr}[N_{\alpha\beta}]$. Finally, to calculate the baryon asymmetry, we multiply N_{B-L}^f by the sphaleron conversion factor and divide by the photon number density, to account for the change between the end of the leptogenesis era and recombination, $\eta_B = a_{\text{sph}}N_{B-L}^f/N_\gamma^{\text{rec}}$ where $a_{\text{sph}} = 12/37$ [32].

4.1 N_1 in Kinetic and Chemical Equilibrium

Having established the density matrix equations which determine the matter-antimatter asymmetry in our setup, we now consider how the temperatures of the two sectors evolve with time, assuming that kinetic and chemical equilibrium can be maintained within the hot sector while N_1 decays (pink stars in fig. 5). We first consider the SM temperature, T_{SM} , and then the hot sector temperature, T_{N_1} .

Before N_1 starts to decay around $T_{N_1} \sim m_{N_1}$, its comoving number density N_{N_1} will remain constant, T_{N_1} will drop as a^{-1} , and the two sectors will remain decoupled. When N_1 starts to decay, the hot sector transfers energy (Q_{N_1}) to the SM sector at a rate

$$\frac{dQ_{N_1}}{dt} = -\frac{dQ_{\text{SM}}}{dt} = -m_{N_1}V \left(\Gamma_{D_1}^0(z_{N_1})N_{N_1} - \Gamma_{D_1}^0(z_{\text{SM}})N_{N_1}^{\text{eq}} \right), \quad (4.5)$$

where we normalise using the volume that contains one photon when we begin tracking the abundances, $V = 1/n_\gamma^{\text{eq}}(a = 1)$. Note that this is exact since the thermally averaged energy transfer rate is $\langle \Gamma_{D_1}^0 m_{N_1} E_{N_1} / E_{N_1} \rangle = m_{N_1} \Gamma_{D_1}^0$. Using eq. (4.1) and $H = \dot{a}/a$ this gives

$$\frac{dQ_{\text{SM}}}{da} = -m_{N_1}V \frac{dN_{N_1}}{da}. \quad (4.6)$$

As the SM sector is in thermodynamic equilibrium, we can apply the second law of thermodynamics to calculate the change in total entropy of the Standard Model,

$$dS_{\text{SM}} = \frac{dQ_{\text{SM}}}{T_{\text{SM}}}, \quad (4.7)$$

and use this to find the evolution of T_{SM} with a . First we write

$$\frac{dS_{\text{SM}}}{da} = \frac{d(s_{\text{SM}}a^3V)}{da}, \quad (4.8)$$

where s_{SM} is the SM sector entropy density, which becomes

$$\frac{1}{T_{\text{SM}}} \frac{dQ_{\text{SM}}}{da} = a^3V \frac{ds_{\text{SM}}}{dT_{\text{SM}}} \frac{dT_{\text{SM}}}{da} + 3a^2V s_{\text{SM}}, \quad (4.9)$$

when we use eq. (4.7) and differentiate the right-hand side. The rate of change of the SM sector entropy density s_{SM} with respect to its temperature is

$$\frac{ds_{\text{SM}}}{dT_{\text{SM}}} = \frac{2\pi^2}{15} g_*(T_{\text{SM}}) T_{\text{SM}}^2 + \frac{2\pi^2}{45} T_{\text{SM}}^3 \frac{dg_*(T_{\text{SM}})}{dT_{\text{SM}}}, \quad (4.10)$$

where numerically we neglect the second term which only has a small change due to N_2 and N_3 . Finally, using eqs. (4.6), (4.9) and (4.10), we find that

$$\frac{dT_{\text{SM}}}{da} = -\frac{15}{2\pi^2 g_* a^3 T_{\text{SM}}^3} \left(m_{N_1} \frac{dN_{N_1}}{da} + 3a^2 s_{\text{SM}} T_{\text{SM}} \right). \quad (4.11)$$

Next, we show how we determine the evolution of T_{N_1} . When N_1 is in kinetic and chemical equilibrium, the solution to eq. (4.1) is the equilibrium comoving number density, which is

$$N_{N_1}^{\text{eq}} = a^3 n_{N_1}^{\text{eq}} V = a^3 V \frac{g_{N_1}}{2\pi^2} T_{N_1}^3 I_+ \left(\frac{m_{N_1}}{T_{N_1}} \right), \quad (4.12)$$

where n_{N_1} is the (non-comoving) number density of N_1 . We account for the quantum statistics of N_1 using

$$I_+(z_{N_1}) = \int_0^\infty d\xi \frac{\xi^2}{\exp[\sqrt{\xi^2 + z_{N_1}^2}] + 1}, \quad (4.13)$$

where $\xi = |\vec{p}_{N_1}|/T_{N_1}$. Thus, for a fixed m_{N_1} there is then a one-to-one relationship between $N_{N_1} = N_{N_1}^{\text{eq}}$ and T_{N_1} , so solving eq. (4.1) tells us how T_{N_1} evolves with a . Equations (4.1) to (4.4), (4.11) and (4.12) then provide a set of coupled differential equations which we solve using the numerical framework of ULYSSES [33, 34]. Once we fix an initial T_{SM} , $\kappa = T_{N_1}/T_{\text{SM}}$ and the comoving number densities, we can use these equations to track N_{N_i} , T_{N_1} , T_{SM} and $N_{\alpha\beta}$ as a function of a , which allows us to compute the final baryon asymmetry η_B . As the scalar ϕ remains in kinetic and chemical equilibrium with N_1 , the hot sector depletes completely as N_1 decays. We do not include the contribution from ϕ in the computation of the asymmetry, since for $2m_{N_1} < m_\phi$ its abundance will be Boltzmann suppressed at the time of N_1 decay. The ϕ population will both mildly increase the generated asymmetry by producing N_1 's as it decays, and mildly decrease it as it dumps entropy into the SM sector.

4.2 N_1 in Kinetic Equilibrium Only

We will now explore regions of the parameter space where number-changing interactions are slower than the Hubble rate, so the assumption of chemical equilibrium no longer holds (green stars in fig. 5). In this case, the density matrix equations, eqs. (4.1) to (4.4), and the SM temperature derivative dT_{SM}/da , eq. (4.11), remain the same as in the previous section. However, the evolution of the temperature of the hot sector, $T_{N_1}(a)$, is no longer given by eq. (4.12), as the lack of number-changing interactions leads to a departure from the equilibrium number density. The phase space distribution function for N_1 is $f_{N_1} = (n_{N_1}/n_{N_1}^{\text{eq}}) f_{N_1}^{\text{eq}}$ where $f_{N_1}^{\text{eq}}$ is the Fermi-Dirac distribution. Approximating the Fermi-Dirac distribution with a Maxwell-Boltzmann distribution, the energy density ρ and pressure p of N_1 become

$$\rho_{N_1} = \left(\frac{n_{N_1}}{n_{N_1}^{\text{eq}}} \right) \rho_{N_1}^{\text{eq}}, \quad (4.14)$$

$$p_{N_1} = \left(\frac{n_{N_1}}{n_{N_1}^{\text{eq}}} \right) p_{N_1}^{\text{eq}}. \quad (4.15)$$

We can now calculate the evolution of T_{N_1} using the second law of thermodynamics and comoving energy conservation. First, we use the second law of thermodynamics,

$$dS_{N_1} = \frac{dQ_{N_1}}{T_{N_1}}, \quad (4.16)$$

to equate

$$\frac{dS_{N_1}}{da} = \frac{ds_{N_1} a^3 V}{da} \quad (4.17)$$

$$= \frac{d}{da} \left(\frac{\rho_{N_1} + p_{N_1}}{T_{N_1}} a^3 V \right) \quad (4.18)$$

$$= \frac{a^3 V}{T_{N_1}} \left(\frac{d\rho_{N_1}}{da} + \frac{dp_{N_1}}{da} - s_{N_1} \frac{dT_{N_1}}{da} + 3 \frac{s_{N_1} T_{N_1}}{a} \right), \quad (4.19)$$

with

$$\frac{1}{T_{N_1}} \frac{dQ_{N_1}}{da} = \frac{m_{N_1} V}{T_{N_1}} \frac{dN_{N_1}}{da}. \quad (4.20)$$

We see that we now require expressions for the rate of change of the energy density of N_1 , $d\rho_{N_1}/da$, and for the rate of change of the pressure of N_1 , dp_{N_1}/da .

To find an expression for $d\rho_{N_1}/da$ we can use the conservation of total comoving energy density,

$$a \frac{d\rho_{\text{tot}}}{da} + 3(\rho_{\text{tot}} + p_{\text{tot}}) = 0, \quad (4.21)$$

where ρ_{tot} and p_{tot} are the total energy density and pressure, respectively. We see that the derivatives of the energy densities in the two sectors are related by

$$a \frac{d\rho_{N_1}}{da} = -3(\rho_{\text{tot}} + p_{\text{tot}}) - a \frac{d\rho_{\text{SM}}}{da}. \quad (4.22)$$

For the rate of change of the pressure, dp_{N_1}/da , we differentiate eq. (4.15) with respect to a to write dp_{N_1}/da in terms of dT_{N_1}/da and dn_{N_1}/da ,

$$\frac{dp_{N_1}}{da} = \frac{n_{N_1}}{n_{N_1}^{\text{eq}}} \frac{dp_{N_1}^{\text{eq}}}{da} + \frac{dn_{N_1}}{da} \frac{p_{N_1}^{\text{eq}}}{n_{N_1}^{\text{eq}}} - \frac{p_{N_1}}{n_{N_1}^{\text{eq}}} \frac{dn_{N_1}^{\text{eq}}}{da} \quad (4.23)$$

$$= \left(\frac{n_{N_1}}{n_{N_1}^{\text{eq}}} \frac{dp_{N_1}^{\text{eq}}}{dT_{N_1}} - \frac{p_{N_1}}{n_{N_1}^{\text{eq}}} \frac{dn_{N_1}^{\text{eq}}}{dT_{N_1}} \right) \frac{dT_{N_1}}{da} + \frac{dn_{N_1}}{da} \frac{p_{N_1}^{\text{eq}}}{n_{N_1}^{\text{eq}}}. \quad (4.24)$$

Together, eqs. (4.19), (4.20), (4.22) and (4.24) give an expression for dT_{N_1}/da in terms of quantities we can compute or track. This, in combination with the density matrix equations, eqs. (4.1) to (4.4), and the T_{SM} evolution equation in the previous section, eq. (4.11), can be solved with the appropriate initial conditions to find the resulting baryon asymmetry. The initial conditions we take for our benchmark point are that N_1 has an equilibrium abundance while N_2 and N_3 have vanishing initial abundance. This is motivated by the possibility that ϕ (or another particle) mediated sufficiently fast number changing rates for N_1 at higher temperatures, but that it no longer can at $T_{N_1} \sim m_{N_1}$. In the case where N_1 is only in kinetic equilibrium with itself around its decay, the ϕ abundance is heavily suppressed and does not contribute to the asymmetry generation (beyond maintaining kinetic equilibrium in the hot sector).

Benchmark	S_1	S_2	S_3	\overline{S}_1	\overline{S}_2	\overline{S}_3	S_4	\overline{S}_4	Our Benchmark
Δ_ν [%]	0.2	0.3	0.2	0.6	0.7	0.4	0.2	0.5	855
Δ_H [%]	0.08	0.02	0.004	0.3	0.06	0.1	0.001	0.007	10.4

Table 1: Degree of fine-tuning for the best-fit points found in Ref. [13] and for our benchmark point (see table 2), using the fine-tuning measures given in appendix B. Smaller numbers indicate a larger degree of fine-tuning, with some degree of fine-tuning for numbers smaller than $\sim 10\%$.

5 Results

Standard non-resonant leptogenesis, which can produce a baryon asymmetry consistent with observations using RHN masses around 10^6 – 10^7 GeV, requires fine-tuning of the light neutrino masses [13] and the SM Higgs mass [10, 12]. The neutrino mass fine-tuning occurs because the tree and one-loop contributions to the light neutrino mass matrix have opposing signs [35] and standard leptogenesis requires them to be separately large and then largely cancel to give an overall small neutrino mass consistent with observation. Fine-tuned solutions are favoured because the specific structure of the R -matrix reduces effective Yukawa couplings, which in turn decreases washout effects and leads to successful leptogenesis, while also enabling this critical cancellation between the tree-level and one-loop contributions, keeping the light neutrino masses within experimental bounds. The SM Higgs mass is also fine-tuned as the RHNs contribute at the one-loop level, with lower RHN masses giving a smaller loop level contribution but also reducing the amount of baryon asymmetry produced.

Using the measures defined in appendix B, the degree of fine-tuning for both the light neutrino mass and the SM Higgs required for successful standard leptogenesis with $m_{N_1} \sim 10^{6.5}$ GeV is given in table 1, based on benchmarks from Ref. [13]. These benchmarks, S_i (\overline{S}_i) for $i = 1, 2, 3, 4$, correspond to normal (inverted) ordering with the PMNS matrix parameters set to their best-fit values based on global data [36]. The remaining CI parameters are fixed to ensure a viable baryon asymmetry. From table 1, we see that the fine-tuning is worse than 1% for both the light neutrino mass and the SM Higgs. We present these benchmarks and their associated tuning measures to evaluate how effectively hot leptogenesis can reduce fine-tuning while still producing the observed baryon asymmetry.

Here we explore two distinct scenarios of hot leptogenesis which alleviate this fine-tuning: one in which N_1 is only in kinetic equilibrium with itself before decay and one in which chemical equilibrium is also established. The parameters that determine whether chemical and kinetic equilibrium are established are different to those that determine the baryon asymmetry (except that they determine the manner of evolution of our model – these scenarios evolve under a different set of evolution equations as described in the previous section). The parameters related to the baryon asymmetry are given in table 2. We will focus on a benchmark scenario for the neutrino parameters, where we use the

Parameter	Unit	Benchmark point
δ	[$^\circ$]	270
α_{21}	[$^\circ$]	50
α_{31}	[$^\circ$]	120
θ_{23}	[$^\circ$]	49.1
θ_{12}	[$^\circ$]	33.41
θ_{13}	[$^\circ$]	8.54
x_1	[$^\circ$]	7
y_1	[$^\circ$]	15
x_2	[$^\circ$]	1
y_2	[$^\circ$]	2
x_3	[$^\circ$]	4
y_3	[$^\circ$]	3
m_1	[eV]	0
$\log_{10}(m_{N_1}/[\text{GeV}])$	[1]	7
$\log_{10}(m_{N_2}/[\text{GeV}])$	[1]	7.006
$\log_{10}(m_{N_3}/[\text{GeV}])$	[1]	7.4
κ	[1]	10

Table 2: Input parameters in the Casas-Ibarra parametrisation for our benchmark point, see text for details.

Casas-Ibarra parametrisation to construct the Yukawa matrix Y [21]. The constrained light neutrino parameters δ , θ_{12} , θ_{13} and θ_{23} are fixed at their best-fit value from recent global fit data [37] where we assume normally ordered light neutrino masses and for simplicity assume the lightest neutrino mass $m_1 = 0$ eV. While we fix the Majorana phases to be 50° and 120° , they do not significantly affect the resulting baryon asymmetry. For the right-handed neutrino masses, we choose an intermediate-mass scale $m_{N_1} \sim 10^7$ GeV, commensurate with the standard case studied in Ref. [13]. We fix m_{N_2} and m_{N_3} to reduce the Higgs fine-tuning measure while ensuring that leptogenesis occurs well beyond the resonant regime (the decay widths of N_1 , N_2 and N_3 are approximately 10^{-5} GeV, 10^{-3} GeV and 10^{-2} GeV, respectively, which are much smaller than the N_1 - N_2 mass splitting of approximately 10^5 GeV). The remaining Casas-Ibarra parameters, x_i and y_i , are chosen to provide a reduced fine-tuning to the light neutrino masses. Finally, the benchmark has an initial ratio of temperatures of $\kappa = T_{N_1}/T_{\text{SM}} = 10$, which gives approximately the maximum achievable baryon asymmetry. We note that if we assumed standard thermal leptogenesis, in the absence of a hot sector, this benchmark point significantly under-produces the baryon asymmetry. We now numerically integrate the evolution equations, show the evolution of various quantities for this benchmark point and investigate the impact of varying one or two parameters at a time on the final baryon asymmetry.

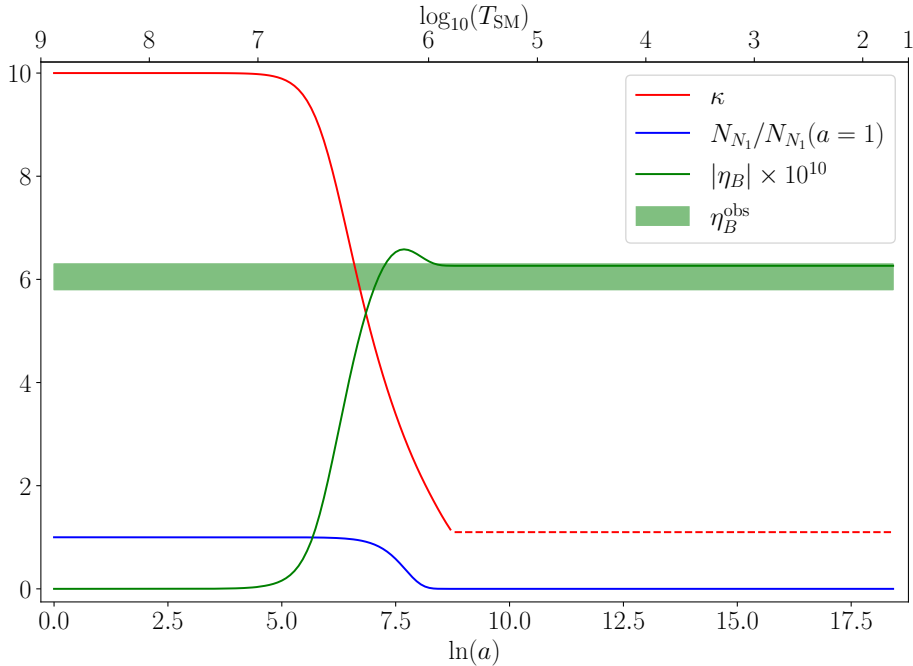


Figure 7: Evolution of $|\eta_B|$, N_{N_1} and κ for initial $\kappa_{\text{in}} = 10$ when N_1 is only in kinetic equilibrium in the hot sector, for our benchmark point. When the number density approaches zero, κ is set to 1 (dashed line). The green band indicates the baryon-to-photon ratio at the 3σ level.

5.1 N_1 in Kinetic Equilibrium Only

We first focus on the case where N_1 is only in kinetic equilibrium with itself. Note that the scenario differs from that considered by Ref. [9], where N_1 is in equilibrium.

In fig. 7 we show the evolution of the temperature ratio κ (red), the number density of the lightest right-handed neutrino N_{N_1} (blue), and the baryon asymmetry η_B (green) as a function of $\ln a$ (where we set $a = 1$ at the beginning of our simulation) for the benchmark point in table 2. We also show the corresponding SM temperature on the top axis. We see that at early times before N_1 has started to decay, at $T_{\text{SM}} \gtrsim 10^7$ GeV and $T_{N_1} \gtrsim 10^8$ GeV, the temperature ratio, the N_1 comoving number density and the baryon asymmetry remain constant. When the N_1 population starts to decay, at $T_{\text{SM}} \sim 10^7$ GeV and $T_{N_1} \sim 10^8$ GeV, the decay starts to put the two sectors into kinetic equilibrium and the temperature ratio κ begins to fall. The baryon asymmetry immediately starts rising and overshoots the observed value around halfway through the decay. It then reduces slightly due to the effect of the washout terms. The temperature ratio approaches $\kappa = 1$ as the hot sector is depleted, and at some point the N_1 abundance goes below the numerical accuracy of our computation. At this point, we set $\kappa = 1$ (dashed red line) so the system can evolve while avoiding numerical errors. This procedure does not affect the final baryon asymmetry η_B as almost all N_1 particles have decayed by this time. Note, however, that even though the two sectors are technically in kinetic equilibrium, the hot sector is essentially empty since almost all N_1

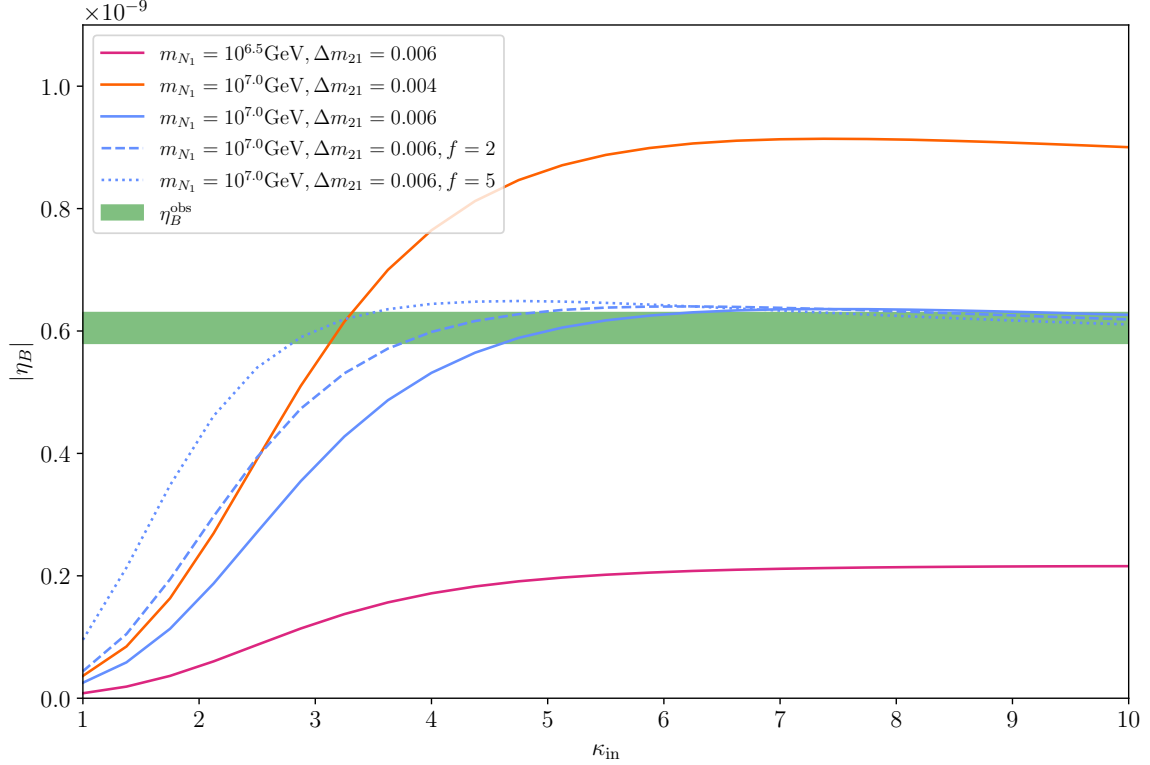


Figure 8: The final baryon asymmetry $|\eta_B|$ as a function of the initial temperature ratio $\kappa_{\text{in}} = T_{N_1}/T_{\text{SM}}$ at $a = 1$. The blue line indicates the benchmark point. In the burgundy and orange curves we vary the RHN mass scale and splittings (see text for details), while the dashed (dotted) blue curves indicate non-equilibrium initial abundances of N_1 , $f \equiv \left(n_{N_1}/n_{N_1}^{\text{eq}}\right)_{\text{in}}$.

particles have decayed. We see that our benchmark point produces a baryon asymmetry within the observed 3σ band. For these parameters we find $\Delta_\eta \approx 855\%$ (indicating that the tree-level mass is $\mathcal{O}(10)$ times larger than the loop level mass) and $\Delta_H \approx 10.4\%$ (indicating that the loop level contribution is $\sim \text{TeV}$) so there is no fine-tuning in the light neutrino masses and very mild fine-tuning in the Higgs mass.

In fig. 8 (blue curve) we show the final baryon asymmetry as a function of the initial temperature ratio κ for our benchmark point. We see that $|\eta_B|$ is far below the observed asymmetry for $\kappa \sim 1$ and first increases with κ . The rate of increase reaches a maximum of around $\kappa = 2.7$, where the energy densities of the SM and N_1 are approximately equal. After this point, the baryon asymmetry begins to level off and reaches a maximum around $\kappa \sim 7$. For $1 \lesssim \kappa \lesssim 7$ the initial number density of N_1 in the hot sector is larger than for $\kappa = 1$, which enhances the final asymmetry. For $2.7 < \kappa$ the hot sector dominates the energy density of the universe, and so the Hubble expansion rate (eq. (3.3)), which counteracts the increased asymmetry. Essentially, the energy dump from the hot sector dilutes the baryon asymmetry. In fig. 8 we also show the impact of varying important parameters. We see that reducing the RHN masses by setting $m_{N_1} = 10^{6.5} \text{ GeV}$ and keeping

the mass splittings fixed (burgundy curve) significantly reduces the generated asymmetry, as is typical in leptogenesis since the Yukawa matrix $Y \propto M_N$. The N_1 – N_2 mass splitting is defined as $\Delta m_{21} = \log_{10}(m_{N_2}/[\text{GeV}]) - \log_{10}(m_{N_1}/[\text{GeV}])$, with Δm_{31} defined analogously and preserved at 0.4. Reducing the right-handed neutrino masses reduces the fine-tuning to $\Delta_H = 58\%$, which is a bit better than our benchmark point, but does not reproduce the observed baryon asymmetry. We also see that a smaller mass splitting between N_1 and N_2 (orange curve) enhances the asymmetry. This also very slightly decreases the amount of fine-tuning needed in the Higgs sector to $\Delta_H = 10.4\%$, because the N_2 state is lighter. When fitting the light neutrino masses, the smaller $N_1 - N_2$ mass splitting leads to a larger $Y_{\mu 1}$ and $Y_{\mu 3}$ and a smaller $Y_{\mu 2}$ (with the other Yukawas remaining approximately constant). Since the $Y_{\alpha 1}$ couplings have the largest impact on the generated asymmetry, this leads to an overall increase. If one wanted to find the minimal fine-tuning possible in this scenario, this could potentially be achieved by reducing the mass splitting further (while remaining out of the resonant leptogenesis regime), which boosts the asymmetry, while reducing the overall RHN mass scale, which reduces the asymmetry and would further improve the fine-tuning in the SM Higgs sector. In the dashed and dotted blue lines, we show the impact of changing the initial N_1 abundance to 2 and 5 times its equilibrium abundance. We see that as the initial abundance increases, the asymmetry increases faster and levels off around a similar maximum value, but at a lower κ_{in} . Increasing the initial abundance is in many ways similar to increasing the hot sector temperature, as both lead to a higher initial number density of N_1 and an increased energy density in the hot sector. While the number and energy densities scale differently with temperature, this does not lead to an increased final asymmetry at large κ_{in} . In fact, for a higher initial abundance, the asymmetry drops slowly at large κ_{in} .

Finally, in fig. 9 we show the baryon asymmetry in y_2 and y_3 , chosen for their impact on the baryon asymmetry. On the left, we show the standard leptogenesis case where $T_{N_1} = T_{\text{SM}}$ and the N_1 are in chemical equilibrium with themselves, while on the right we show the results for hot leptogenesis with an initial $\kappa = 10$ and where N_1 particles are only in kinetic equilibrium with themselves. The benchmark point is indicated by a red cross. In the left panel, we see that in this region of parameter space standard leptogenesis under-produces the baryon asymmetry by more than an order of magnitude. In the right panel, we see that η_B is enhanced by a factor of ~ 50 compared to the standard case and the observed baryon asymmetry can be produced in this parameter space (the dashed green contours give the 3σ range). Importantly, this is away from the regime in the top-right where Higgs-mediated $N_1\ell \rightarrow N_1\ell$ and lepton-mediated $N_1H \rightarrow N_1H$ elastic scattering processes equilibrate the SM and the hot sector, indicated by the greyed-out ‘Thermalisation’ region. The fine-tuning in both the Higgs mass and the neutrino masses do not depend strongly on the parameters y_2 and y_3 so remain approximately equal to those of the benchmark point.

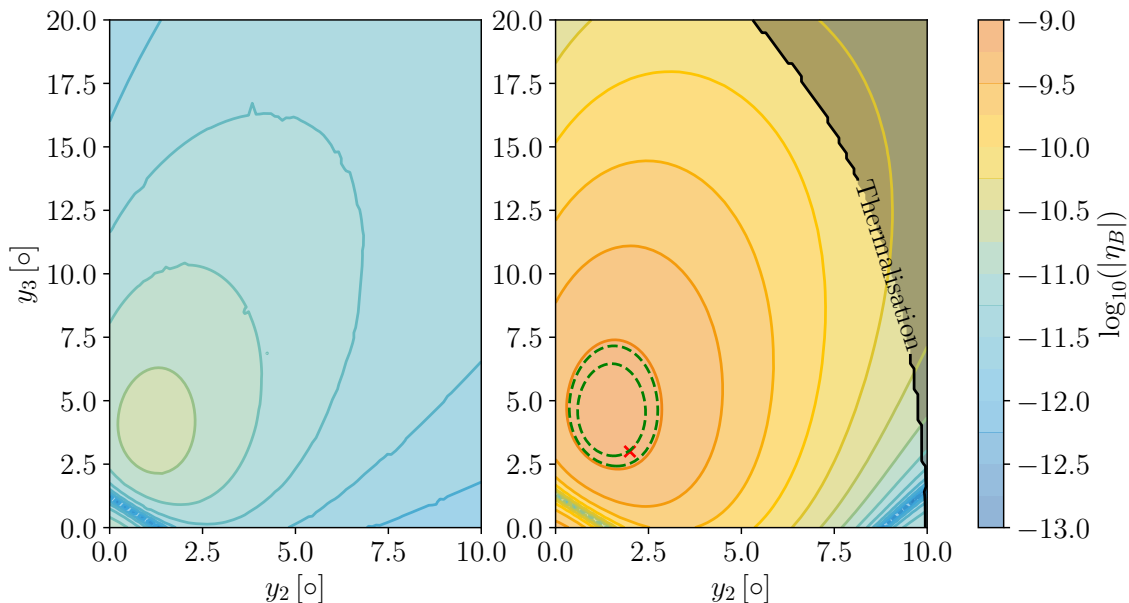


Figure 9: Values of η_B for standard leptogenesis (left) and hot leptogenesis (right) for $\kappa_{\text{in}} = 10$ produced with the RHN in kinetic equilibrium only. The green dashed contours corresponding to η_B produced at $(5.8 - 6.3) \times 10^{-10}$ [38, 39] and the red cross indicates our benchmark point. The greyed-out region represents when the non-thermalisation assumption no longer holds, such that hot leptogenesis may not be viable. $\Delta_H \sim 10.4\%$ and $\Delta_\nu \sim 855\%$ throughout the plot.

5.2 N_1 in Kinetic and Chemical Equilibrium

We now briefly turn to the scenario where the hot sector is in both kinetic and chemical equilibrium with itself. As described above, in this scenario we assume $n_{N_1} = n_{N_1}^{\text{eq}}$ throughout and use this relation to find the evolution of the hot sector temperature T_{N_1} .

Even though we are in a different region of parameter space, pink stars in fig. 5, these parameters do not strongly impact the N_1 evolution and baryon asymmetry generation, which depend on the parameters in table 2. Taking the initial N_1 abundance to be $N_{N_1}^{\text{eq}}$ and using the benchmark parameters in table 2, we find that the κ , N_{N_1} and η_B evolution is virtually identical to fig. 7. For this reason, we do not show it, but instead just show the results of a parameter scan in y_2 and y_3 in fig. 10. We see that the difference with fig. 9 is very small: at most a factor 4 in the baryon asymmetry near the thermalisation region, but at the percent level in the region where the observed η_B is produced. The thermalisation region has moved slightly to the left, indicating that it is easier for the hot sector to come into kinetic equilibrium with the SM sector in this scenario. The fine-tuning, in this case, is identical to that in section 5.1.

Overall, we see that phenomenologically it does not make a significant difference whether only kinetic equilibrium, or both kinetic and chemical equilibrium, are maintained during N_1 decay. Both scenarios can produce the observed baryon asymmetry while

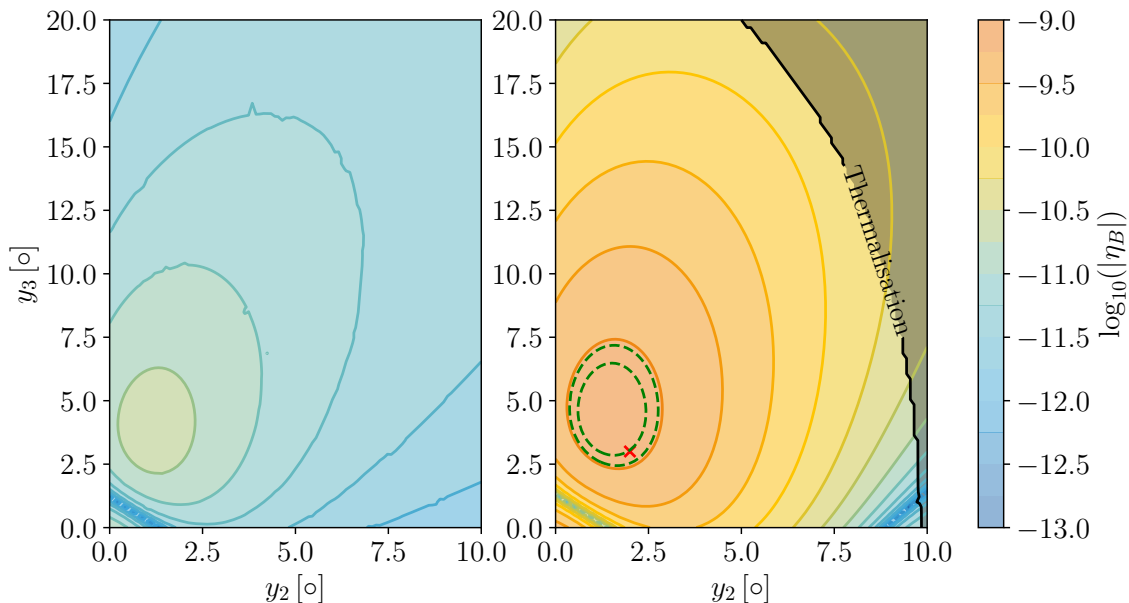


Figure 10: Values of η_B for standard leptogenesis (left) and hot leptogenesis (right) for $\kappa_{\text{in}} = 10$ produced with the RHN in kinetic and chemical equilibrium. The green dashed contours corresponding to η_B produced at $(5.8 - 6.3) \times 10^{-10}$ [38, 39] and the red cross indicates our benchmark point. The greyed out region represents when the non-thermalisation assumption no longer holds, such that hot leptogenesis may not be viable. $\Delta_H \sim 10.4\%$ and $\Delta_\nu \sim 855\%$ throughout the plot.

avoiding fine-tuning of the neutrino masses or the SM Higgs mass.

5.3 Further Scenarios

We now briefly comment on two possible alternative scenarios. First, kinetic equilibrium could be established after inflaton decay but not maintained in the hot sector while N_1 decays. This could, for example, occur if a heavy mediator realises fast $2N_1 \rightarrow 2N_1$ scattering shortly after inflaton decay, but is too heavy to maintain it at $T_{N_1} \sim m_{N_1}$. In this scenario, one in principle has to compute the evolution for the full set of momentum modes. However, in the absence of additional processes affecting the sector, the assumption of a thermal distribution may be reasonable until the N_1 start to decay. As was shown in [40], in vanilla leptogenesis the assumption of kinetic equilibrium when it is not realised underestimates the final baryon asymmetry by a tiny amount, because low momentum N_1 particles are more efficiently produced than accounted for in a thermal distribution. In our present scenario, we may expect that large momentum N_1 particles decay earlier, and thus the produced asymmetry is overestimated by a small amount if kinetic equilibrium is assumed.

Second, there is the possibility of N_2 and N_3 starting with temperature at or around T_{N_1} and with an approximately equilibrium abundance, but where all three particles are

weakly coupled and do not establish kinetic equilibrium with the SM. While Ref. [9] shows that the observed light neutrino masses mean that, in a type-I see-saw scenario, the decay rate of N_2 and N_3 must be larger than Hubble at temperatures around their masses, we find that they do not have enough time to fully equilibrate before decay. It is therefore possible that this scenario may lead to an asymmetry which is larger by up to a factor of three compared to the results we find here, further reducing the required fine-tuning.

6 Conclusions

In this work, we have studied a class of leptogenesis scenarios in which the sector containing the lightest right-handed neutrino (N_1) establishes kinetic equilibrium with itself at a temperature higher than that of the Standard Model (SM) sector. We have motivated this setup by considering the decay of the inflaton, which can lead to two sectors with similar but distinct temperatures. Higher temperatures in the N_1 sector enhance the number density of N_1 particles and can lead to an enhanced baryon asymmetry. With this setup, the observed baryon asymmetry can be generated without the significant fine-tuning of the light neutrino masses and the SM Higgs boson mass present in standard leptogenesis. We have checked that inflaton-mediated energy exchange between the sectors is not fast enough to equilibrate them after inflation.

In section 3 we described a toy model that can realise such a scenario of hot leptogenesis, introducing a new scalar field ϕ responsible for mediating self-interactions of N_1 and maintaining its kinetic equilibrium. We explore two regimes: one where the hot sector containing N_1 is only in kinetic equilibrium with itself and another where it is in both kinetic and chemical equilibrium. We derived the relevant evolution equations to track the relevant quantities and compute the resulting baryon asymmetry in both of these scenarios.

Our numerical analysis reveals that both scenarios can produce the observed baryon asymmetry with minimal fine-tuning. As expected, the enhancement of the baryon asymmetry can be up to a factor of around 50, and the observed asymmetry can then be achieved for smaller right-handed neutrino masses and couplings. These scenarios therefore reduce the fine-tuning required in both the Higgs and neutrino sectors compared to the standard leptogenesis scenario. This confirms that non-resonant leptogenesis is viable and efficient in producing the observed baryon asymmetry under our model assumptions.

Comparing the numerical results in the two cases, we find that the results for kinetic only and kinetic and chemical equilibrium are similar. This can be understood from the fact that we assume $n_{N_1} = n_{N_1}^{\text{eq}}$ as an initial condition for the former case, which is preserved until $T \sim m_{N_1}$, right before the decays happen. Thus, we expect that chemical equilibrium can be a reasonable approximation in the case where it is not realised or maintained.

We finally note that our computations are also likely to be a good approximation to the case where N_1 are not in kinetic equilibrium with themselves when they decay and that it may be possible that N_2 and N_3 are present in the hot sector and could lead to an enhanced baryon asymmetry.

Acknowledgments

AB, DC and JT are supported by the STFC under Grant No. ST/T001011/1. MJB and DC acknowledge support from Royal Society International Exchanges grant IESR1221078. MJB also acknowledges support from the University of Massachusetts Amherst, the DIVA Program at the IPPP Durham University, and is grateful to the IPPP for their hospitality during the completion of this work.

A Cross-Sections, Decay Rates and Thermal Averaging

In this appendix, we give details of the cross-sections, decay rates and thermal averaging we use in our computations.

A.1 Cross-Sections and Decay Rates

In section 3 we examine a number of processes that contribute to energy exchange (via elastic scattering) or particle number exchange (via number-changing processes). Here, we give the relevant cross-sections which we calculated with the help of `FeynCalc` [41].

The Feynman diagrams for the elastic scattering processes $N_1 N_{2,3} \rightarrow N_1 N_{2,3}$ are given in fig. 4 (a) and (b), and the cross-section is

$$\begin{aligned} \sigma_{N_1 N_{2,3} \rightarrow N_1 N_{2,3}}(s) = & \frac{(y_\phi^1)^2 (y_\phi^{2,3})^2}{4\pi m_\phi^2 s^2 (m_\phi^2 + s)} \left[s \left(4m_{N_1}^2 \left(4m_{N_{2,3}}^2 - m_\phi^2 \right) + m_\phi^2 \left(2m_\phi^2 - 4m_{N_{2,3}}^2 + s \right) \right) \right. \\ & \left. + 2m_\phi^2 (m_\phi^2 + s) \left(m_\phi^2 - 2 \left(m_{N_1}^2 + m_{N_{2,3}}^2 \right) \right) \log \left(\frac{m_\phi^2}{m_\phi^2 + s} \right) \right], \quad (\text{A.1}) \end{aligned}$$

where s is the squared centre-of-mass energy. This process is relevant for considering whether the SM and hot sectors come into equilibrium via elastic scattering.

Figure 4 (a), (b) and (c) contribute to the elastic scattering process $N_1 N_1 \rightarrow N_1 N_1$, leading to the cross-section

$$\begin{aligned} \sigma_{2N_1 \rightarrow 2N_1}(s) = & \frac{(y_\phi^1)^4}{16\pi s^2 m_\phi^2 (m_\phi^2 - s)^2 (m_\phi^2 + s) (2m_\phi^2 + s)} \left[m_\phi^2 (m_\phi^4 - s^2) (24m_{N_1}^4 (s - 2m_\phi^2) \right. \\ & + 16m_{N_1}^2 (5s^2 + 2m_\phi^2 s - 4m_\phi^4) + 16m_\phi^6 - 8m_\phi^4 s - 5m_\phi^2 s^2) \log \left(\frac{m_\phi^2}{m_\phi^2 + s} \right) \\ & + s(2m_\phi^2 + s) (16m_{N_1}^4 (6m_\phi^4 - 9m_\phi^2 s + 5s^2) - 8m_{N_1}^2 (4m_\phi^6 - 9m_\phi^4 s + 7m_\phi^2 s^2) \\ & \left. + 8m_\phi^8 - 12m_\phi^6 s + 3m_\phi^4 s^2 + 3m_\phi^2 s^3) \right]. \quad (\text{A.2}) \end{aligned}$$

This process can maintain kinetic equilibrium in the hot sector.

Now we will consider number-changing processes that can maintain chemical equilibrium. The decay rate for $\phi \rightarrow 2N_1$ shown in fig. 6 (a) in the ϕ rest frame is given by

$$\Gamma_{\phi \rightarrow 2N_1}^0 = \frac{(y_\phi^1)^2 (m_\phi^2 - 4m_{N_1}^2)^{\frac{3}{2}}}{8\pi m_\phi^2}. \quad (\text{A.3})$$

The cross-section for $2N_1 \rightarrow 2\phi$ shown in fig. 6 (b) and (c) is

$$\begin{aligned} \sigma_{2N_1 \rightarrow 2\phi}(s) = & \frac{y_\phi^4}{64\pi s (s - 4m_{N_1}^2)} \left[- \frac{2\sqrt{s - 4m_{N_1}^2} \left(16m_{N_1}^4 + 2m_{N_1}^2 (s - 8m_\phi^2) + 3m_\phi^4 \right)}{m_{N_1}^2 \sqrt{s - 4m_\phi^2 + m_\phi^4}} \right. \\ & \left. + \frac{\left(s^2 - 4m_\phi^2 s + 6m_\phi^4 - 32m_{N_1}^4 + 16m_{N_1}^2 (s - m_\phi^2) \right)}{(s - 2m_\phi^2)} \log \left(\frac{\sqrt{(s - 4m_{N_1}^2) (s - 4m_\phi^2) - 2m_\phi^2 + s}}{\sqrt{(s - 4m_{N_1}^2) (s - 4m_\phi^2) + 2m_\phi^2 - s}} \right) \right]. \end{aligned} \quad (\text{A.4})$$

The cross-section for the s -channel process $2N_1 \rightarrow 3\phi$ shown in fig. 6 (d) is [42]

$$\begin{aligned} \sigma_{2N_1 \rightarrow 3\phi}(s) = & \frac{\lambda^2 m_{N_1}^2 y_\phi^2}{6144\pi^2 s^2 (m_\phi - \sqrt{s})^2 (m_\phi + \sqrt{s})^{3/2}} \sqrt{\frac{s(3m_\phi - \sqrt{s})}{s - 4m_{N_1}^2}} \\ & \left[(m_\phi + \sqrt{s})(3m_\phi^2 + s)\tilde{E}(m_\phi, s) - (m_\phi - \sqrt{s})^2(3m_\phi + \sqrt{s})\tilde{F}(m_\phi, s) \right], \end{aligned} \quad (\text{A.5})$$

where $\tilde{E}(m_\phi, s)$ is defined as

$$\tilde{E}(m_\phi, s) = E \left(\arcsin \left(\frac{1}{4} \sqrt{\frac{(3m_\phi - \sqrt{s})(m_\phi + \sqrt{s})^3}{m_\phi^3 \sqrt{s}}} \right), \frac{16m_\phi^3 \sqrt{s}}{(3m_\phi - \sqrt{s})(m_\phi + \sqrt{s})^3} \right), \quad (\text{A.6})$$

and $E(x, y)$ is the incomplete elliptic integral of the second kind, and similarly for $\tilde{F}(m_\phi, s)$ where $F(x, y)$ is the incomplete elliptic integral of the first kind and the arguments are related in the same way.

A.2 Thermal Averaging

For the rates considered in section 3.1 we need the thermally averaged cross-sections for the initial states $2N_1$ and $N_1 N_{2,3}$, where N_1 and $N_{2,3}$ are at different temperatures.

The thermal averaged cross-section for two identical incoming N_1 particles is given in Ref. [43],

$$\langle \sigma v \rangle = \frac{1}{8m_{N_1}^4 T_{N_1} K_2^2 \left(\frac{m_{N_1}}{T_{N_1}} \right)} \int_{4m_{N_1}^2}^{\infty} ds \sigma(s) (s - 4m_{N_1}^2) \sqrt{s} K_1 \left(\frac{\sqrt{s}}{T_{N_1}} \right), \quad (\text{A.7})$$

where K_1 and K_2 are modified Bessel functions of the first and second kind, respectively.

For two incoming particles of different masses and different temperatures, we generalise the results in Refs. [43–45]. For the case of the initial state $N_1 N_2$, the thermal average is given by

$$\langle \sigma \bar{v} \rangle = \frac{\int \sigma \bar{v} f_{N_1} f_{N_2} d^3 \mathbf{p}_{N_1} d^3 \mathbf{p}_{N_2}}{\int f_{N_1} f_{N_2} d^3 \mathbf{p}_{N_1} d^3 \mathbf{p}_{N_2}} \quad (\text{A.8})$$

where \bar{v} is the Møller velocity. We then neglect quantum statistics and take the approximation that f_{N_1} and f_{N_2} are given by Maxwell-Boltzmann distributions. This assumption lets us perform the integrals analytically and introduces minimal errors in our results. We first compute the denominator,

$$\int f_{N_1} f_{N_2} d^3 \mathbf{p}_{N_1} d^3 \mathbf{p}_{N_2} = 16\pi^2 T_{N_1} T_{\text{SM}} m_{N_1}^2 m_{N_2}^2 K_2 \left(\frac{m_{N_1}}{T_{N_1}} \right) K_2 \left(\frac{m_{N_2}}{T_{\text{SM}}} \right), \quad (\text{A.9})$$

where we have used the fact that $E dE = |\mathbf{p}| d|\mathbf{p}|$ to rewrite the integral. For the numerator we follow the computation in [46]. We change coordinates from E_{N_1} and E_{N_2} to $x_{\pm} = \frac{E_N}{T_{N_1}} \pm \frac{E_{N_2}}{T_{\text{SM}}}$, where the upper limit of the x_- integration is

$$x_-^{\text{max}} = \frac{m_{N_1}^2 T_{\text{SM}}^2 x_+ + \sqrt{(m_{N_1}^2 - s)^2 T_{\text{SM}} \left(m_{N_1}^2 (T_{N_1} - T_{\text{SM}}) + T_{\text{SM}} (T_{N_1} T_{\text{SM}} x_+^2 - s) \right)}}{m_{N_1}^2 T_{\text{SM}} (T_{\text{SM}} - T_{N_1}) + s T_{N_1}}. \quad (\text{A.10})$$

Integration over x_- and x_+ then leads to

$$\langle \sigma \bar{v} \rangle = D \int_{(m_{N_1} + m_{N_2})^2}^{\infty} ds \sigma(s) \frac{C}{B} \left(A(1+z)e^{-z} + C\sqrt{B}K_1(z) \right) \quad (\text{A.11})$$

where

$$A = m_{N_1}^2 T_{\text{SM}}^2 - m_{N_2}^2 T_{N_1}^2 \quad (\text{A.12})$$

$$B = m_{N_2}^2 T_{N_1} (T_{N_1} - T_{\text{SM}}) + m_{N_1}^2 T_{\text{SM}} (T_{\text{SM}} - T_{N_1}) + s T_{N_1} T_{\text{SM}} \quad (\text{A.13})$$

$$C = \sqrt{(s - (m_{N_1} - m_{N_2})^2)(s - (m_{N_1} + m_{N_2})^2)} \quad (\text{A.14})$$

$$D^{-1} = 8m_{N_1}^2 m_{N_2}^2 K_2 \left(\frac{m_{N_1}}{T_{N_1}} \right) K_2 \left(\frac{m_{N_2}}{T_{\text{SM}}} \right), \quad (\text{A.15})$$

$$z = \frac{\sqrt{B}}{T_{N_1} T_{\text{SM}}}. \quad (\text{A.16})$$

The thermally averaged cross-section for initial states $N_1 N_3$ is given by replacing N_2 with N_3 .

B Fine-Tuning

To quantify the degree of fine-tuning present in the neutrino sector, we will adopt a fine-tuning measure that is the inverse of that used in [13]. The matrix of physical light neutrino masses M_ν is

$$M_\nu = M_\nu^{\text{tree}} + M_\nu^{\text{1-loop}}, \quad (\text{B.1})$$

where M_ν^{tree} contains the tree-level Lagrangian neutrino masses and $M_\nu^{\text{1-loop}}$ is the one loop contribution (which is always negative) [13]. The fine-tuning can be measured using,

$$\Delta_\nu = \frac{\sum_{i=1}^3 \text{SVD}[M_\nu]_i}{\sum_{i=1}^3 \text{SVD}[M_\nu^{\text{1-loop}}]_i}, \quad (\text{B.2})$$

where SVD is the Singular Value Decomposition of the matrix, i.e., $\text{SVD}[M]_i$ is the square root of the i -th (real and positive) eigenvalue of M^*M . If the eigenvalues of M are real and positive, then the singular value decomposition of M simply gives the eigenvalues. Fine-tuning of $\Delta_\nu \approx 1\%$ corresponds to, e.g., $M_\nu^{\text{tree}} \approx 100M_\nu$ and $M_\nu^{\text{1-loop}} \approx 100M_\nu$, so the tree and loop level masses would cancel to one part in 100.

Analogously for the Higgs sector, we will have

$$\mu_H^2 \approx (\mu_H^{\text{tree}})^2 - |\delta\mu^2|, \quad (\text{B.3})$$

where $\mu_H = \frac{m_h}{\sqrt{2}} = 88 \text{ GeV}$ is the effective Higgs mass parameter, μ_H^{tree} is the Lagrangian Higgs parameter and $\delta\mu^2$ is the one-loop correction to the Higgs mass parameter [10],

$$|\delta\mu^2| \approx \frac{1}{4\pi^2} \text{Tr} [Y M_N^2 Y^\dagger]. \quad (\text{B.4})$$

The degree of fine-tuning in the mass parameters (not the mass squared parameters) can be measured with

$$\Delta_H = \sqrt{\frac{(\mu_H^{\text{tree}})^2 - |\delta\mu^2|}{\frac{1}{2}((\mu_H^{\text{tree}})^2 + |\delta\mu^2|)}} \approx \sqrt{\frac{\mu_H^2}{|\delta\mu^2|}}, \quad (\text{B.5})$$

where we have assumed $\mu_H^2 \ll (\mu_H^{\text{tree}})^2, |\delta\mu^2|$. Fine-tuning of $\Delta_H = 10\%$ corresponds to $|\delta\mu| = 10\mu_H = 880 \text{ GeV}$.

References

- [1] P. Minkowski, $\mu \rightarrow e\gamma$ at a Rate of One Out of 10^9 Muon Decays?, *Phys. Lett. B* **67** (1977) 421.
- [2] T. Yanagida, Horizontal gauge symmetry and masses of neutrinos, *Conf. Proc. C* **7902131** (1979) 95.
- [3] M. Gell-Mann, P. Ramond and R. Slansky, Complex Spinors and Unified Theories, *Conf. Proc. C* **790927** (1979) 315 [[1306.4669](#)].
- [4] R.N. Mohapatra and G. Senjanovic, Neutrino Mass and Spontaneous Parity Nonconservation, *Phys. Rev. Lett.* **44** (1980) 912.
- [5] M. Fukugita and T. Yanagida, Baryogenesis Without Grand Unification, *Phys. Lett. B* **174** (1986) 45.
- [6] L. Covi, E. Roulet and F. Vissani, CP violating decays in leptogenesis scenarios, *Phys. Lett. B* **384** (1996) 169 [[hep-ph/9605319](#)].
- [7] L. Covi and E. Roulet, Baryogenesis from mixed particle decays, *Phys. Lett. B* **399** (1997) 113 [[hep-ph/9611425](#)].

- [8] A. Pilaftsis, CP violation and baryogenesis due to heavy Majorana neutrinos, *Phys. Rev. D* **56** (1997) 5431 [[hep-ph/9707235](#)].
- [9] N. Bernal and C.S. Fong, Hot Leptogenesis from Thermal Dark Matter, *JCAP* **10** (2017) 042 [[1707.02988](#)].
- [10] J.D. Clarke, R. Foot and R.R. Volkas, Electroweak naturalness in the three-flavor type I seesaw model and implications for leptogenesis, *Phys. Rev. D* **91** (2015) 073009 [[1502.01352](#)].
- [11] S. Davidson and A. Ibarra, A Lower bound on the right-handed neutrino mass from leptogenesis, *Phys. Lett. B* **535** (2002) 25 [[hep-ph/0202239](#)].
- [12] F. Vissani, Do experiments suggest a hierarchy problem?, *Phys. Rev. D* **57** (1998) 7027 [[hep-ph/9709409](#)].
- [13] K. Moffat, S. Pascoli, S.T. Petcov, H. Schulz and J. Turner, Three-flavored nonresonant leptogenesis at intermediate scales, *Phys. Rev. D* **98** (2018) 015036 [[1804.05066](#)].
- [14] A. Pilaftsis and T.E.J. Underwood, Resonant leptogenesis, *Nucl. Phys. B* **692** (2004) 303 [[hep-ph/0309342](#)].
- [15] G. Lazarides and Q. Shafi, Origin of matter in the inflationary cosmology, *Phys. Lett. B* **258** (1991) 305.
- [16] G.F. Giudice, M. Peloso, A. Riotto and I. Tkachev, Production of massive fermions at preheating and leptogenesis, *JHEP* **08** (1999) 014 [[hep-ph/9905242](#)].
- [17] T. Asaka, K. Hamaguchi, M. Kawasaki and T. Yanagida, Leptogenesis in inflaton decay, *Phys. Lett. B* **464** (1999) 12 [[hep-ph/9906366](#)].
- [18] T. Asaka, K. Hamaguchi, M. Kawasaki and T. Yanagida, Leptogenesis in inflationary universe, *Phys. Rev. D* **61** (2000) 083512 [[hep-ph/9907559](#)].
- [19] V.N. Senoguz and Q. Shafi, GUT scale inflation, nonthermal leptogenesis, and atmospheric neutrino oscillations, *Phys. Lett. B* **582** (2004) 6 [[hep-ph/0309134](#)].
- [20] F. Hahn-Woernle and M. Plumacher, Effects of reheating on leptogenesis, *Nucl. Phys. B* **806** (2009) 68 [[0801.3972](#)].
- [21] J.A. Casas and A. Ibarra, Oscillating neutrinos and $\mu \rightarrow e, \gamma$, *Nucl. Phys. B* **618** (2001) 171 [[hep-ph/0103065](#)].
- [22] J.M. Cline, K. Kainulainen and K.A. Olive, Protecting the primordial baryon asymmetry from erasure by sphalerons, *Phys. Rev. D* **49** (1994) 6394 [[hep-ph/9401208](#)].
- [23] B. Garbrecht and P. Schwaller, Spectator Effects during Leptogenesis in the Strong Washout Regime, *JCAP* **10** (2014) 012 [[1404.2915](#)].
- [24] M. Hufnagel and M.H.G. Tytgat, The domain of a cannibal dark matter, *JCAP* **09** (2023) 012 [[2212.09759](#)].
- [25] A. Ghosh, S. Gope and S. Mukhopadhyay, Cannibal dark matter decoupled from the standard model: Cosmological constraints, *Phys. Rev. D* **106** (2022) 103515 [[2206.11046](#)].
- [26] R. Barbieri, P. Creminelli, A. Strumia and N. Tetradis, Baryogenesis through leptogenesis, *Nucl. Phys. B* **575** (2000) 61 [[hep-ph/9911315](#)].
- [27] A. Abada, S. Davidson, F.-X. Josse-Michaux, M. Losada and A. Riotto, Flavor issues in leptogenesis, *JCAP* **04** (2006) 004 [[hep-ph/0601083](#)].

- [28] A. De Simone and A. Riotto, On the impact of flavour oscillations in leptogenesis, *JCAP* **0702** (2007) 005 [[hep-ph/0611357](#)].
- [29] S. Blanchet, P. Di Bari and G.G. Raffelt, Quantum Zeno effect and the impact of flavor in leptogenesis, *JCAP* **0703** (2007) 012 [[hep-ph/0611337](#)].
- [30] S. Blanchet, P. Di Bari, D.A. Jones and L. Marzola, Leptogenesis with heavy neutrino flavours: from density matrix to Boltzmann equations, *JCAP* **1301** (2013) 041 [[1112.4528](#)].
- [31] A. Abada, S. Davidson, A. Ibarra, F.X. Josse-Michaux, M. Losada and A. Riotto, Flavour Matters in Leptogenesis, *JHEP* **09** (2006) 010 [[hep-ph/0605281](#)].
- [32] M. D’Onofrio, K. Rummukainen and A. Tranberg, Sphaleron Rate in the Minimal Standard Model, *Phys. Rev. Lett.* **113** (2014) 141602 [[1404.3565](#)].
- [33] A. Granelli, K. Moffat, Y. Perez-Gonzalez, H. Schulz and J. Turner, Ulysses: Universal leptogenesis equation solver, *Computer Physics Communications* **262** (2021) 107813.
- [34] A. Granelli, C. Leslie, Y.F. Perez-Gonzalez, H. Schulz, B. Shuve, J. Turner et al., ULYSSES, universal LeptogeneSiS equation solver: Version 2, *Comput. Phys. Commun.* **291** (2023) 108834 [[2301.05722](#)].
- [35] J. Lopez-Pavon, S. Pascoli and C.-f. Wong, Can heavy neutrinos dominate neutrinoless double beta decay?, *Phys. Rev. D* **87** (2013) 093007 [[1209.5342](#)].
- [36] I. Esteban, M.C. Gonzalez-Garcia, M. Maltoni, I. Martinez-Soler and T. Schwetz, Updated fit to three neutrino mixing: exploring the accelerator-reactor complementarity, *JHEP* **01** (2017) 087 [[1611.01514](#)].
- [37] I. Esteban, M.C. Gonzalez-Garcia, M. Maltoni, T. Schwetz and A. Zhou, The fate of hints: updated global analysis of three-flavor neutrino oscillations, *JHEP* **09** (2020) 178 [[2007.14792](#)].
- [38] T.-H. Yeh, J. Shelton, K.A. Olive and B.D. Fields, Probing physics beyond the standard model: limits from BBN and the CMB independently and combined, *JCAP* **10** (2022) 046 [[2207.13133](#)].
- [39] P.D. Group, R.L. Workman, V.D. Burkert, V. Crede, E. Klempt, U. Thoma et al., Review of Particle Physics, *Progress of Theoretical and Experimental Physics* **2022** (2022) 083C01 [<https://academic.oup.com/ptep/article-pdf/2022/8/083C01/49175539/ptac097.pdf>].
- [40] F. Hahn-Woernle, M. Plumacher and Y.Y.Y. Wong, Full Boltzmann equations for leptogenesis including scattering, *JCAP* **08** (2009) 028 [[0907.0205](#)].
- [41] V. Shtabovenko, R. Mertig and F. Orellana, New Developments in FeynCalc 9.0, *Comput. Phys. Commun.* **207** (2016) 432 [[1601.01167](#)].
- [42] J.C.R. ao, Integration of three body phase space: The 3BodyXSections and 3BodyDecays packages, .
- [43] P. Gondolo and G. Gelmini, Cosmic abundances of stable particles: Improved analysis, *Nucl. Phys. B* **360** (1991) 145.
- [44] J. Edsjö and P. Gondolo, Neutralino relic density including coannihilations, *Physical Review D* **56** (1997) 1879–1894.
- [45] M. Cannoni, Relativistic $\langle \sigma v_{\text{rel}} \rangle$ in the calculation of relics abundances: a closer look, *Phys. Rev. D* **89** (2014) 103533 [[1311.4494](#)].

- [46] A. Cheek, L. Heurtier, Y.F. Perez-Gonzalez and J. Turner, Primordial black hole evaporation and dark matter production. ii. interplay with the freeze-in or freeze-out mechanism, [Physical Review D **105** \(2022\)](#) .